

---

Electronic Thesis and Dissertation Repository

---

10-9-2018 10:00 AM

## 7T Magnetic Resonance Spectroscopy of Non-Lesional Temporal Lobe Epilepsy

John Robert Adams  
*The University of Western Ontario*

Supervisor  
Bartha, Robert  
*The University of Western Ontario*

Graduate Program in Medical Biophysics  
A thesis submitted in partial fulfillment of the requirements for the degree in Master of Science  
© John Robert Adams 2018

Follow this and additional works at: <https://ir.lib.uwo.ca/etd>



Part of the [Investigative Techniques Commons](#)

---

### Recommended Citation

Adams, John Robert, "7T Magnetic Resonance Spectroscopy of Non-Lesional Temporal Lobe Epilepsy" (2018). *Electronic Thesis and Dissertation Repository*. 5760.  
<https://ir.lib.uwo.ca/etd/5760>

This Dissertation/Thesis is brought to you for free and open access by Scholarship@Western. It has been accepted for inclusion in Electronic Thesis and Dissertation Repository by an authorized administrator of Scholarship@Western. For more information, please contact [wlsadmin@uwo.ca](mailto:wlsadmin@uwo.ca).

## Abstract

Temporal lobe epilepsy (TLE) is the most common form of focal epilepsy, and one that is generally amenable to surgical treatment when surgery is necessary. Unfortunately, roughly 25-30% of the patient population have no visible lesions on clinical MRI scans. Without anatomical abnormalities to help guide surgical resection, the success of surgical treatment decreases substantially. However, metabolic abnormalities may exist that could allow for accurate localization of epileptic tissue in this cohort. Magnetic resonance spectroscopy (MRS) is a technique that can detect and measure the concentration of metabolically important molecules within tissue, giving insight into the underlying cellular metabolism.

In this thesis, non-lesional TLE patients were studied and compared with control subjects using single voxel MRS at a magnetic field strength of 7T for the first time. We hypothesized that metabolite changes in the hippocampus would be associated with seizure lateralization. Non-lesional patients showed altered levels of creatine and choline when compared to healthy controls. These results were in agreement with prior work in the literature showing non-lesional TLE is primarily a result of glial cell proliferation without neuronal atrophy. However, in the patient cohort studied, these metabolites did not effectively lateralize seizure origin, potentially due to the varied underlying pathologies within the patient group.

**Keywords:** *Epilepsy, Temporal Lobe Epilepsy, Magnetic Resonance Spectroscopy, Magnetic Resonance Imaging, 7T, Choline*

## Co-Authorship

The following thesis contains material from posters that have been previously presented at a number of conferences and will be submitted for publication in the near future. The contributions of other co-authors are listed below. The author of this thesis acquired the majority of the presented data, assisted in developing the necessary data analysis software, performed all data analysis, and prepared the relevant presentations and manuscripts.

A portion of the material presented in Chapter 2 was presented at the Imaging Network of Ontario's 2018 Symposium and the International Society for Magnetic Resonance in Medicine's 2018 Annual General Meeting in Paris. Co-authors for this work were Simona Nikolova, who acquired the first eight patient and control datasets and performed initial data analysis; Suzan Brown, who was responsible for patient recruitment and clinical data management; Dickson Wong, who developed the data analysis software used; and Drs. Robert Bartha and Jorge Burneo, who conceptualized the study and provided project oversight and guidance all stages of this work.

## Acknowledgements

I want to thank the many people who made this thesis possible and who helped me through the duration of my masters; for me the time has flown by, and I have all of you to thank.

Firstly, I want to thank my supervisor, Dr. Bartha for his constant guidance and support throughout the duration of my time in his lab. I would also like to thank the other members of the Bartha lab and the students and staff working at CFMM for their help and advice. In particular I would like to thank Dickson Wong and Amy Schranz, for their help developing the tools needed to analyze the presented data along with their troubleshooting advice.

On the clinical side of my research project, I want to thank Dr. Jorge Burneo for his help and guidance in planning and organising my research project, and Suzan Brown, our research coordinator, for her tireless help with patient recruitment and managing patient information.

My thanks to The Canada First Research Excellence Fund and the Epilepsy Program of the Ontario Brain Institute for their ongoing funding of this project.

Last but not least, I want to thank my friends and family for their constant moral support, especially my parents Robert and Colleen.

# Table of Contents

<b>Abstract</b>	<b>i</b>
<b>Co-Authorship</b>	<b>ii</b>
<b>Acknowledgements</b>	<b>iii</b>
<b>List of Figures</b>	<b>vi</b>
<b>List of Tables</b>	<b>vii</b>
<b>List of Symbols and Abbreviations</b>	<b>viii</b>
<b>1 Introduction</b>	<b>1</b>
1.1 Research objectives	2
1.2 Epilepsy	2
1.2.1 The Temporal Lobe	3
1.2.2 Neurotransmission	4
1.2.3 Epileptogenesis and Epilepsy Risk Factors	13
1.2.4 Treatment	13
1.3 Magnetic Resonance	17
1.3.1 Classical Electromagnetism	17
1.3.2 NMR – A Proton’s Perspective	19
1.3.3 Excitation	21
1.3.4 Signal Detection	22
1.3.5 Relaxation	22
1.3.6 Gradients	24
1.3.7 Magnetic Resonance Spectroscopy	26
1.4 Spectroscopy in Temporal Lobe Epilepsy	38
1.4.1 Creatine	38
1.4.2 <i>N</i> -Acetylaspartate	39
1.4.3 Choline	40
1.4.4 Glutamate and Glutamine	41
1.4.5 <i>Myo</i> -Inositol	42
1.5 Thesis Outline	43
References	44
<b>2 7T Magnetic Resonance Spectroscopy of the Hippocampus in Non-Lesional Temporal Lobe Epilepsy</b>	<b>51</b>
2.1 Introduction	52
2.2 Methods	54
2.2.1 Patient Recruitment	54

2.2.2	Seizure Lateralization	56
2.2.3	MR Protocol	56
2.2.4	Spectral Processing and Metabolite Quantification	58
2.2.5	Statistical Analysis	60
2.3	Results	63
2.3.1	Group Analysis	63
2.3.2	Asymmetry Analysis	63
2.4	Discussion	66
2.5	Conclusions	69
	References	70
<b>3</b>	<b>Conclusions and Future Work</b>	<b>75</b>
3.1	Conclusions	76
3.2	Future Work	77
	References	79
<b>A</b>	<b>Ethics Approval</b>	<b>80</b>
A.1	Ethics Approval for Human Epilepsy study	81
	<b>Curriculum Vitae</b>	<b>82</b>

## List of Figures

1.1	Lobes of the Human Brain	5
1.2	Anatomy of the Mesial Temporal Lobe	5
1.3	T <sub>1</sub> - and T <sub>2</sub> -weighted Images of Hippocampal Sclerosis	6
1.4	Labeled Diagram of a Neuron	7
1.5	Simple Pulse Sequences Illustrating Relaxation Effects	25
1.6	Fit 7T semi-LASER Spectrum Collected from the Hippocampus	29
1.7	Example J-coupling Multiplets	30
1.8	The semi-LASER Pulse Sequence	37
2.1	Hippocampal Voxel Placement	57

## List of Tables

2.1	Patient Demographics and MRS Asymmetry Results	55
2.2	Relaxation Times used in Absolute Metabolite Quantification	61
2.3	Metabolite Levels Within Subject Groups and $p$ -values from MANCOVA Analysis	64
2.4	Average Metabolite Asymmetry Scores and Lateralization Results	65



## List of Symbols and Abbreviations

${}^1\text{H}$	Proton
$\omega$	Larmor frequency
$\gamma$	Gyromagnetic ratio
ADP	Adenosine diphosphate
AED	Anti-epileptic drug
AFP	Adiabatic full passage pulse
AI	Asymmetry index
ATP	Adenosine triphosphate
$B_0$	Externally applied magnetic field
$B_1(t)$	Magnetic field from RF coil
$\text{Ca}^{2+}$	Calcium ions
Cho	Choline
$\text{Cl}^{1-}$	Chlorine ions
CNS	Central nervous system
Cr	Creatine
CSF	Cerebral spinal fluid
EEG	Electroencephalography
$E_M(\theta)$	Magnetic potential energy
FDG-PET	Fluorodeoxyglucose positron emission tomography
GABA	$\gamma$ -Aminobutyric acid
Gln	Glutamine
Glu	Glutamate
Glx	Combined glutamate and glutamine
GM	Grey matter (brain tissue)
GSH	Glutathione
$\text{K}^+$	Potassium ions

LASER	Localization by adiabatic selective refocusing pulse sequence
MANCOVA	Multivariate analysis of covariance
MRE	Medically refractory epilepsy
MRI	Magnetic resonance imaging
MRS	Magnetic resonance spectroscopy
MRSI	Magnetic resonance spectroscopic imaging
Myo	<i>Myo</i> -inositol
$M_{XY}$	Transverse magnetization
$M_Z$	Longitudinal magnetization
Na <sup>+</sup>	Sodium ions
NAA	<i>N</i> -acetylaspartate
NMR	Nuclear magnetic resonance physics
PCr	Phosphocreatine
ppm	Parts-per-million
RF	Radio frequency
semi-LASER	Semi- localization by adiabatic selective refocusing pulse sequence
SNR	Signal-to-noise ratio
SPECT	Single-photon emission computed tomography
SUDEP	Sudden unexpected death in epilepsy
$T_1$	Longitudinal relaxation
$T_2$	Transverse relaxation
$T_2^*$	Observed transverse relaxation
TE	Echo time
TLE	Temporal lobe epilepsy
TR	Relaxation time
WM	White Matter (brain tissue)

# **Chapter 1**

## **Introduction**

## 1.1 Research Motivation and Objectives

The motivation for the work presented in this thesis was to improve surgical outcomes for patients with drug resistant temporal lobe epilepsy and normal appearing clinical MRI scans. In drug resistant epilepsy, surgical removal of seizure forming tissue is the most common method of treatment. However localization of seizure focus is often difficult in patients without visible disease markers on MRI, due to the poor localization abilities of other techniques such as electroencephalography (EGG) and clinical semiology. Uncertainty in the location of seizure origin has been shown to reduce the success rate of epilepsy surgery, largely because some seizure forming tissue can be missed in the resection. To address this issue, magnetic resonance spectroscopy (MRS) was explored in this thesis as a technique to non-invasively identify and localize epileptic tissue in pre-surgical planning. Metabolite changes measured by MRS are indicative of altered tissue metabolism, and may be changed by seizure activity in the absence of MRI visible lesions. These MRS measurements were performed in this patient population for the first time at a magnetic field strength of 7T, with the goal of demonstrating that additional information can be gleaned from these measurements at 7T and to establish the clinical utility of the method.

## 1.2 Epilepsy

Epilepsy is described by the International League Against Epilepsy as, "... A diverse family of disorders, having in common an abnormally increased predisposition to seizures." [1] Seizures themselves are transient events where neurons within the cortex begin firing out of control in a highly synchronous manner. The outward manifestations of a seizure vary dramatically from patient to patient based on where in the brain a seizure starts and how the seizure spreads throughout the cortex. These outward manifestations include potential symptoms such as behavioural arrest, loss of

consciousness, mood changes, and uncontrolled muscle contractions or spasms. Seizures can have a particularly devastating effect on a patient's quality of life as loss of awareness and/or bodily control at unpredictable times robs many patients of their ability to function independently [1]. Furthermore, epilepsy is associated with a wide range of long term effects and comorbidities such as cognitive deficits (especially memory deficits) and mood disorders such as depression [2], [3]. Those with epilepsy are also at a significantly increased risk for sudden unexpected death (SUDEP) [4], and they are at risk for developing status epilepticus; a condition where the brain's inhibitory mechanisms cannot bring a seizure under control, leading to a prolonged seizure that can cause permanent brain damage or death [5].

From a clinical perspective, epilepsy is commonly divided into two subtypes, focal and generalized epilepsy. Focal epilepsy describes a condition where a patient's seizures consistently arise from specific unilateral regions within the brain, whereas generalized epilepsy describes patients where the seizure onset involves activation of large regions in both hemispheres simultaneously [6]. Within this classification scheme, temporal lobe epilepsy (TLE) is the most common form of focal epilepsy [7]–[9].

### **1.2.1 The Temporal Lobe**

The temporal lobe is one of the primary divisions of the cerebrum; it lies near the base of the skull beneath the Sylvian fissure (Figure 1.1). The temporal lobes are functionally important for their role in the consolidation of memory and in forming speech. In the study of epilepsy, the mesial temporal lobe is particularly important (Figure 1.2). This region consists of a folded grey matter structure known as the hippocampus and nearby regions of cortical grey matter within the hippocampal gyrus. It receives highly processed sensory information from many disparate regions of the brain, and is responsible for consolidating working memory into long-term declarative

memory (facts and experiences). The mesial temporal lobe is the most common site of origin for temporal lobe seizures. Hippocampal sclerosis (hardening and atrophy of the hippocampus) has been the most common cause of epilepsy in this patient group; over 57% of patients with drug-resistant TLE have clear hippocampal sclerosis on MRI (Figure 1.3) [10]–[12].

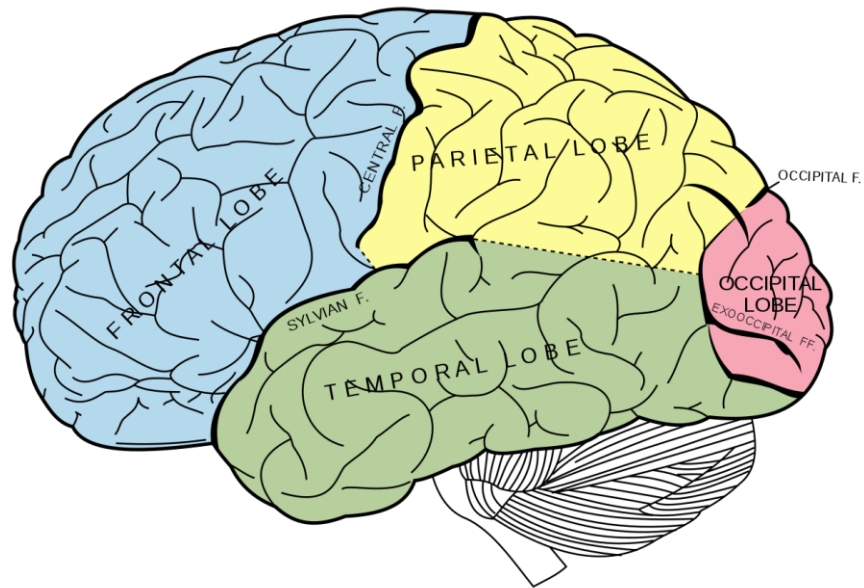
## **1.2.2 Neurotransmission**

To understand epilepsy and the pathophysiology involved, it is important to understand the basic construction of the central nervous system (CNS). The two primary cell types composing the CNS are neurons and glial cells [10].

### **1.2.2.1 Neurons**

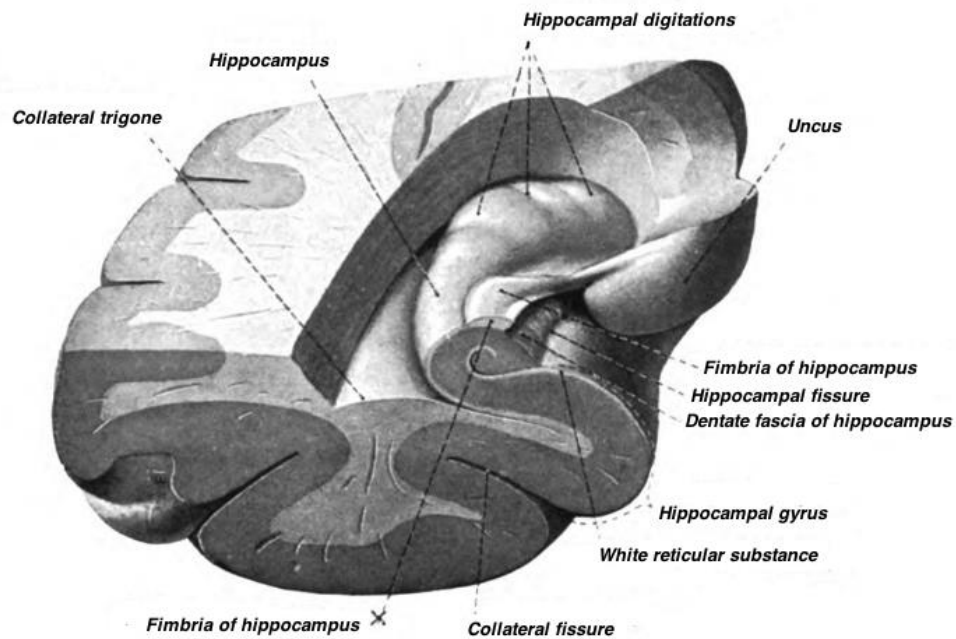
Neurons are the fundamental building blocks of the nervous system. A neuron is composed of a main cell body with numerous branches of varying lengths extending from this central core (Figure 1.4). Typically, a neuron will have a single main branch extending off the cell body, termed the axon, and numerous smaller branches, termed dendrites. Neurons receive a combination of electrical and/or chemical signals through interfaces across its surface called synapses, and transmit information away from the cell body along the axon, which in turn is connected to other neurons. When describing the transmission of signals between two neurons, a neuron that is sending signals are often referred to as the pre-synaptic neuron, while the neuron receiving signal from the pre-synaptic neuron is referred to as the post-synaptic neuron.

Neurons come in a wide range of shapes and sizes based on their function. Neurons used to connect the central nervous system to distant anatomical regions can be over a metre in length, while neurons within different parts of



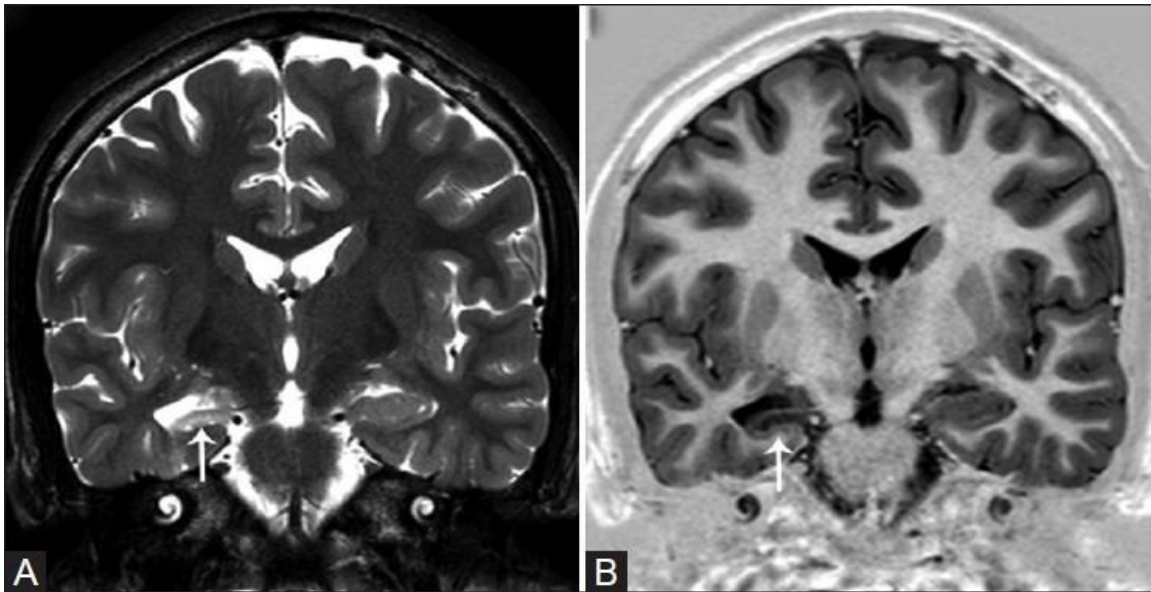
**Figure 1.1 - Lobes of the Human Brain**

Image by Henry Vandyke Carter and Henry Gray [13] [Public Domain], accessed via Wikimedia Commons



**Figure 1.2 - Anatomy of the Mesial Temporal Lobe**

Image by Dr. Johannes Sobotta [14] [Public Domain], accessed via Wikimedia Commons



**Figure 1.3 – T<sub>1</sub>- and T<sub>2</sub>-weighted Images of Hippocampal Sclerosis:** Image showing T<sub>2</sub>-weighted (A) and T<sub>1</sub>-weighted (B) images of an epileptic patient with unilateral right hippocampal sclerosis (arrow). Note the increase in T<sub>2</sub> signal, tissue atrophy, and loss of internal structure in the sclerotic hippocampus as compared to the healthy contralateral hippocampus.

Image by K. Ganesan and M. Ursekar [15], [Licensed for non-commercial use under CC-BY-NC-SA 3.0 (<https://creativecommons.org/licenses/by-nc-sa/3.0/>)], accessed via the Indian Journal of Radiology and Imaging



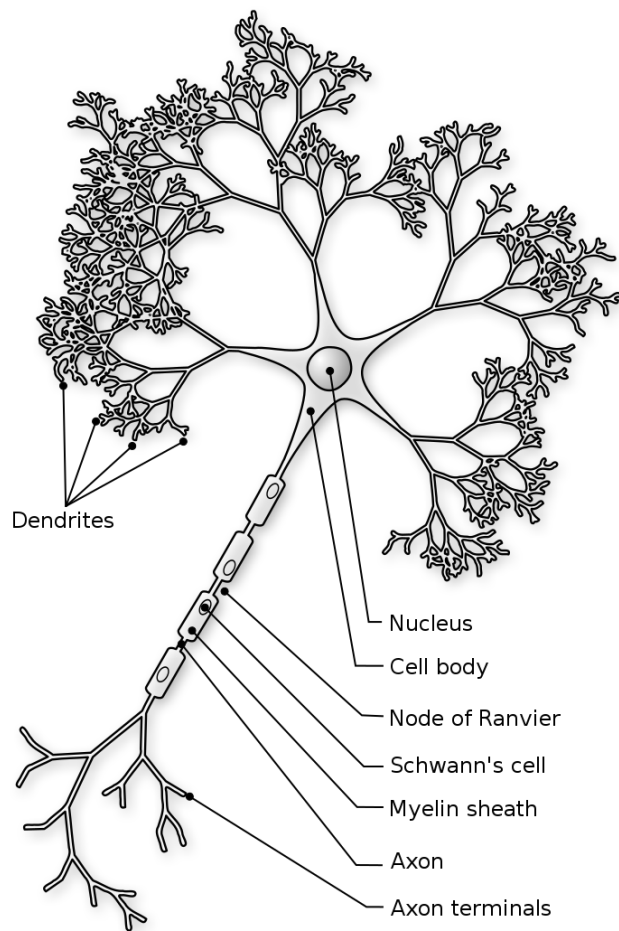


**Figure 1.4 - Labeled Diagram of a Neuron**

Image by Nicholas Rougier  
[Licensed under CC-BY-SA 3.0  
(<http://creativecommons.org/licenses/by-sa/3.0>), accessed via Wikimedia Commons

the CNS take on varied configurations. Throughout the body, neurons are networked together to form neural circuits that can store and process information [10].

### 1.2.2.2 The Action Potential

A neuron is able to convey information along its length in the form of an electrical signal known as the action potential. The action potential itself is generated by the neuron selectively allowing aqueous sodium, calcium and potassium ions ( $\text{Na}^+$ ,  $\text{Ca}^{2+}$ , and  $\text{K}^+$ ) from the surrounding environment to diffuse into or out of the cell, creating an electric current that propagates along the cell. Once the action potential reaches a synapse with another cell it can be transmitted between neurons through a number of different mechanisms.

Prior to the beginning of an action potential, a neuron maintains a 'resting potential' of -65 mV. It is able to maintain this potential due to the action of ion pumps embedded within the cell membrane that selectively pump sodium and calcium ions out of the cell while pumping potassium ions into the cell. This creates concentration gradients that are exploited to generate the action potential. As other neurons send signals to a neuron, they transfer positively charged ions to the dendrites of the post-synaptic neuron. This transfer of charge is accomplished either by directly allowing ions to flow between cells through protein channels which bridge the synaptic cleft, or via the release of chemical signalling molecules known as neurotransmitters which open ion channels on the post-synaptic cell.

Once the local cell membrane reaches a potential of -40 mV, voltage gated sodium channels on the post-synaptic membrane open, allowing a large influx of positively charged  $\text{Na}^+$  ions to diffuse into the cell. These channels remain open for  $\sim 1$  ms before closing and locking shut. As the membrane continues to

depolarize, voltage gated potassium channels open allowing  $K^+$  to rapidly diffuse out of the cell, repolarizing the membrane until it is slightly more negative than the resting potential. With both the sodium and potassium channels closed, the aforementioned sodium-potassium pumps on the cell membrane can restore ion concentrations both within and outside the cell to their original state. This process creates the action potential waveform. An action potential takes about 2 ms to play out, followed by 1 ms refractory period during which the voltage-gated channels are locked closed and the neuron cannot fire. As the cell membrane goes through this firing cycle on the dendrites, it changes the electric potential of the surrounding membrane causing it to also undergo this process. In this way, the action potential travels from the dendrites, through the cell body, to the connection between the neuronal cell body and the axon, known as the axonal hillock. This region of the neuron acts as a signal integrator, collecting all signals received by the dendrites and cell body. If the sum total of all signals received by the neuron are enough to depolarize the axonal hillock, it will generate an action potential which will propagate down the axon and be transmitted to downstream neurons [10], [16].

It is worth noting that the process for generating an action potential described above simply covers neurotransmission between two neurons. Many specialized types of neurons, particularly in sensory organs such as the eyes or skin, can generate an action potential through a variety of mechanisms beyond what is described above. That said, all neurons communicate using action potentials, regardless of the means used to generate them [10].

### 1.2.2.3 Excitation and Inhibition

Neural circuits contain both excitatory neurons and inhibitory neurons; these two neuronal classes are distinguished by the effects they have on the post-synaptic neurons they synapse with.

Excitatory neurons are the more common of the two; these neurons either directly or indirectly transfer positive charge to downstream neurons, bringing them closer to generating an action potential. This is achieved through two methods; direct transmission of the action potential or through the release of neurotransmitters. In direct transmission, ion channels embedded within the pre- and post-synaptic sides of a synapse directly bridge the two neurons, allowing charged ions to flow between the two cells. When an action potential reaches a synapse, ion flow directly transfers the action potential across the synapse allowing it to continue propagating in the post-synaptic neuron. Indirect excitation is performed through neurotransmitter release. When the action potential reaches a synapse, it causes neurotransmitter filled vesicles to bind to the cellular membrane at the synapse and release the neurotransmitter into the synaptic cleft. In the mammalian CNS, the main excitatory neurotransmitter is the molecule glutamate (Glu). The released neurotransmitters then bind to gated ion channels on the post-synaptic cell membrane, opening them and allowing positive ions to flow into the neuron.

Inhibitory neurons function similarly to excitatory neurons, with the key difference being the neurotransmitters they release. Inhibitory neurons primarily use the neurotransmitter  $\gamma$ -aminobutyric acid (GABA). When released into the synaptic cleft, GABA primarily acts on chlorine channels that allow negatively charged  $\text{Cl}^{-1}$  into the postsynaptic neuron. This hyperpolarizes the post-synaptic neuron below the resting potential, making it more difficult for it to generate an action potential. In the healthy brain,

inhibition is used to prevent excitation of unneeded neurons within or adjacent to a network, and to synchronize neuronal activity. It is also important to note that GABA has a complex effect on neurons, and that under certain circumstances it can also have a net excitatory effect on a neuron [10], [17], [18].

#### **1.2.2.4 The Role of Glial Cells**

In addition to the neurons themselves, the CNS is composed of a diverse family of cells collectively known as glial cells. These cells are responsible for both protecting the neurons, and ensuring neurotransmission can occur efficiently through a variety of mechanisms. Most importantly related to this thesis, one type of glial cell known as the astrocyte works with neurons to maintain the chemical environment needed for effective neurotransmission. Astrocytes wrap around the synapses that connect neurons, and take up any neurotransmitters released into the synapse. Once inside the astrocyte, neurotransmitters can be broken down and their components transported back to the neuron, where the neurotransmitter can be resynthesized as needed. The most important example of this is the glutamate-glutamine-GABA cycle, where glutamate that has been used for neurotransmission is taken up by astrocytes and converted into glutamine. Glutamine can then either transferred back to excitatory neurons to resynthesize glutamate, or the astrocyte can convert glutamine into GABA for distribution to inhibitory neurons [10], [19].

#### **1.2.2.5 Neurotransmission and Epilepsy**

In epilepsy, the process of neurotransmission and action potential generation is altered. Epilepsy ultimately results from an imbalance of excitation and inhibition within a neuronal network. This imbalance can be caused by dysfunction at any point in the process of neurotransmission, including

under-expression, over-expression, or malformations of various ion channels that result in abnormal ion flow. These alterations create inhibitory neurons that require extra stimulation to fire and excitatory neurons that easily fire with minimal stimulation. Dysfunction of the astrocytes can also prevent glutamate from being cleared from the synaptic cleft, allowing glutamate to persistently allow positive charge into a neuron after the initial action potential has been generated. Dysfunction of both neurons and astrocytes can cause deregulation of the surrounding chemical environment, which can prevent normal ion flow from repolarizing a neuron after excitation, and can cause GABA to switch from having a net inhibitory to a net excitatory effect [17]–[22].

While the mechanisms can vary greatly, the net effect is much the same; the imbalance of excitation and inhibition creates a positive feedback loop in the effected areas of cortex. Some neurons will begin to fire in a continuous or hyper-synchronous manner, which rapidly propagates throughout the surrounding network. Without appropriate inhibition, positive feedback loops within the normal neural circuitry allow this abnormal firing to both reinforce itself and propagate throughout the brain, preventing normal brain function [11], [12], [23]. Under healthy conditions, neurons that fire together develop stronger connections to one another through a variety of mechanisms regulating protein expression within their synaptic connections. Seizures stimulate these same processes, creating long-term changes that predispose the affected neuronal circuitry to generate additional seizures in the future. If neurons continue to fire over a prolonged seizure, excess intracellular concentrations of ions such as  $\text{Ca}^{2+}$  create a neurotoxic environment, resulting in neuron damage and death as well as proliferation of glial cells such as astrocytes. This damage to cerebral tissue results in long-term cognitive deficits and visible lesions in epileptic patients [5].

### **1.2.3 Epileptogenesis and Epilepsy Risk Factors**

Epileptogenesis, or the process by which seizure forming tissue regions develop and grow, is a complex topic that is still not fully understood. As stated in the ILAE definition of epilepsy, the term ‘epilepsy’ covers a wide range of diseases and disorders that cause seizures [1]. Generally speaking any insult to or malformation of the brain can lead to epileptogenesis, with the main causes being traumatic brain injury, cerebral tumours, viral or parasitic infections, malformations of the brain during development, and genetic mutations that alter the various cellular systems used to generate and regulate action potentials. The precise causes and mechanisms fuelling epileptogenesis are highly variable between patients; understanding how and why these processes develop is an active area of research [23].

Also important to note is that epileptogenesis is an ongoing process. While the early stages of epileptogenesis are difficult to study in humans, because the process begins prior to a patient’s first seizure, it is known that the location and extent of seizure forming tissue can grow and evolve over time as seizures damage tissue and the brain responds to that damage. This ongoing change is important to consider from a clinical perspective, as patients with epilepsy can become more or less difficult to treat over time [1]. At present, epileptogenic processes cannot be reversed by existing epilepsy treatments. Evidence shows certain treatments can alter the development of epilepsy to reduce its severity in select circumstances, but there is no general anti-epileptogenic treatment that would be a true cure for epilepsy [23].

### **1.2.4 Treatment**

When assessing epileptic patients, neurologists assess several risk factors that provide clues about the underlying pathology causing epileptogenesis,

which can be used to guide treatment. These questions include any history of head injury, whether the patient suffered from a provoked seizure (such as a febrile seizure in infancy), and any family history of epilepsy that would suggest a genetic component to the patient's condition.

The primary method for treating epilepsy is the use of anti-epileptic or anti-seizure drugs (AEDs). These pharmacological treatments make use of a variety of treatment pathways; most stimulate the brain's inhibitory pathways to counter the increase in neural excitability that causes seizures. AEDs are effective at controlling seizures for approximately 70% of patients diagnosed with epilepsy, with varied effectiveness based on the type of epilepsy syndrome [9], [24]. If a patient has tried two or more AED's which have failed to adequately control their seizures, or if those drugs did control their seizures but with unacceptable side effects, then clinicians will diagnose that patient with a drug-resistant form of epilepsy [25].

For patients with drug-resistant epilepsy, there are few treatment options available to them. Some forms of juvenile epilepsy can be controlled by the use of a ketogenic diet, however the efficacy of this diet in controlling adult epilepsy is still an area of active research. The predominant treatment for drug resistant patients is neurosurgery. A neurostimulation device is sometimes used, but the more common treatment is resective surgery to disconnect or remove seizure-forming regions from the rest of the brain [25].

#### **1.2.4.1 Electroencephalography in Epilepsy**

Electroencephalography (EEG) is a technique that uses electrodes to record electrical activity in the brain. In a typical scalp EEG measurement, a network of electrodes is placed at standardized positions around the head, using a conductive gel to improve electrical conductivity between the skin and the electrodes. As discussed above, neurons communicate using electrical



currents; as neurons fire they create a change in voltage that is detected by an EEG system. By comparing the difference in voltage between different electrodes, brain activity can be localized to specific regions. Due to the low voltage of the current generated by neurons, combined with the interference created by the various layers of tissue and bone between the brain and the scalp electrodes, EEG requires hundreds of millions of neurons to fire simultaneously to generate detectable signal. Furthermore, the limited current makes it challenging for scalp EEG to detect electrical activity in deeper brain structures. EEG is very good at identifying changes in electrical activity over time, but only gives general information as to where that activity is occurring [10], [26].

EEG, when paired with video monitoring, is the gold standard for diagnosing a patient with epilepsy. During an epileptic seizure, neurons begin firing with an unnatural level of synchronicity; this results in rapid, high amplitude changes in the EEG signal from regions affected by the seizure. Meanwhile, most epileptic patient EEGs show what are known as interictal discharges; abnormalities in EEG signal that suggest that a group of neurons have begun to fire with the synchronicity found in a seizure, but without the development of a seizure or any effects on patient behaviour [1], [26].

As discussed in more detail below, EEG is a key tool in the planning of epilepsy surgery. In addition to traditional scalp EEG, epileptologists will often use invasive EEG techniques, requiring either subdural or depth electrodes. These invasive techniques work on the same principles as scalp EEG, however the electrodes are surgically inserted into the cranial cavity to increase sensitivity and remove the interference created by the skull and other intervening tissues. Subdural electrodes consist of a strip of electrodes inserted between the skull and brain across areas of interest, whereas depth

electrodes consist of a series of electrodes embedded in a needle-like rod, which is then inserted into the brain structures under examination [26].

#### **1.2.4.2 Pre-Surgical Planning in Epilepsy**

The success of resective surgery is highly dependant on accurate localization of epileptic foci to ensure that all seizure forming tissue is removed while simultaneously avoiding damage to functionally normal tissue. This localization process is a multi-modal process utilizing a combination of seizure semiology, EEG recordings, neuropsychological examination, and magnetic resonance imaging (MRI). When additional diagnostic information is needed, fluorodeoxyglucose positron emission tomography (FDG-PET), and single-photon emission computed tomography (SPECT) are added to the armamentarium of tools used to localize epileptogenic focus. Good surgical outcomes are more likely for patients for whom all these techniques converge on single clear site of dysfunction. In patients with ambiguous localization, or seizures that emerge independently from different regions, surgery can still have positive effects. Unfortunately, in these cases it is less likely to completely stop their seizures because epileptic tissue that is part of the focus can be missed in the first resection, allowing it to continue generating seizures [25]–[28].

Typical surgical planning relies most heavily on EEG (often paired with video recordings to capture seizure semiology simultaneously with electrographic recordings) and MRI. EEG confirms the diagnosis of epilepsy and provides general localization of abnormal neuronal activity, while MRI provides imaging data to identify the extent of the abnormal tissue and help identify the underlying disease [27]. However, 20-30% of the epileptic population, depending on the type of epilepsy, have normal appearing clinical MRI scans that do not display any identifiable indicators of tissue abnormality. In these cases, FDG-PET and SPECT may be used to help localize dysfunctional

tissue, however these techniques have their limitations. FDG-PET has high spatial resolution, but gives no information on the underlying cause of the seizures. In addition, the hypometabolic anomalies associated with epilepsy on FDG-PET imaging extend well beyond the seizure focus, limiting localization utility. Meanwhile, while SPECT scans can identify epileptic foci using cerebral blood flow measures, SPECT results have poorer resolution and reliability than FDG-PET [28].

In an attempt to fill this gap in epilepsy treatment, we are evaluating the use of magnetic resonance spectroscopy in presurgical planning; it is known that the biochemical properties of the brain are altered in epileptic regions, and it is hoped that a spectroscopic biomarker could be used to identify the extent of epileptic tissue in MR-normal patients.

### 1.3 Magnetic Resonance

Nuclear magnetic resonance (NMR) is a phenomenon that arises from the magnetic properties of certain atomic nuclei. NMR phenomena can be described using either classical electromagnetism or quantum mechanics; while quantum mechanics gives a more complete explanation of NMR effects, for almost all cases the quantum scenario simplifies to the same results as the classical explanation. The following explanation of NMR effects will detail the classical approach to NMR, using the formulations detailed in [29]–[31]. In the mathematical notation, vector quantities will be denoted in **bolded** text.

#### 1.3.1 Classical Electromagnetism

In general, a movement of electrical charge will generate a magnetic field. For any object that generates a magnetic field, we can describe the magnetic field produced by using that object's magnetic moment  $\boldsymbol{\mu}$ :

$$\boldsymbol{\mu} = \frac{q}{2m} \mathbf{L} = \gamma \mathbf{L} \quad (1.1)$$

where  $q$  is the electric charge of the object,  $m$  is that object's mass,  $\mathbf{L}$  is the angular momentum of the object, and  $\gamma$  is a quantity known as the gyromagnetic ratio. If we were to place this magnetic object within a uniform magnetic field  $\mathbf{B}_0$ , it would experience a torque  $\tau$  according to Equation 1.2:

$$\tau = |\boldsymbol{\mu}| |\mathbf{B}_0| \sin\theta \quad (1.2)$$

where  $\theta$  is the angle between  $\boldsymbol{\mu}$  and  $\mathbf{B}_0$ . This torque would cause the magnetic moment to precess around  $\mathbf{B}_0$  with an angular frequency  $\omega$  determined by Equation 1.3:

$$\omega = \gamma B_0 \quad (1.3)$$

For an idealized magnetic moment in a vacuum, this precession would continue indefinitely. In a more realistic scenario, dissipative forces will act on the magnetic object, causing it to lose the kinetic energy associated with precession until the object reaches an equilibrium position where potential energy is minimized:

$$E_M(\theta) = -\boldsymbol{\mu} \cdot \mathbf{B}_0 = -|\boldsymbol{\mu}| |\mathbf{B}_0| \cos\theta \quad (1.4)$$

The torque produced by the externally applied magnetic field vanishes when the magnetic moment aligns parallel or anti-parallel to  $\mathbf{B}_0$  ( $\theta = 0^\circ$  or  $180^\circ$ ). If we now introduce a network of identical magnetic moments all within the same external  $\mathbf{B}_0$ , the magnetic moments will align with  $\mathbf{B}_0$ . By summing the magnetic field produced by these magnetic moments, we can describe a net magnetic field that is generated by the network.

In principle, this effect is what occurs in an NMR experiment; the nuclei of interest that are present within the sample generate their own magnetic moments, which are then aligned to an external magnetic field. The scale at

which NMR occurs complicates this picture. At the level of atomic nuclei, thermal energy becomes a major complicating factor that prevents the neat alignment of each nuclear magnetic moment along the applied magnetic field. Instead, the applied magnetic field gives the otherwise randomly distributed magnetic moments a slight bias to point along  $\mathbf{B}_0$  (which, by convention, is oriented along the  $z$ -axis). To explore this further we will examine the NMR behaviour of a hydrogen nucleus.

### 1.3.2 NMR – A Proton’s Perspective

As noted above, magnetic moments arise from a movement of charge. A hydrogen nucleus ( $^1\text{H}$ ) is composed of a single proton, and that proton has a quantum spin angular momentum. While the details of quantum spin are beyond the scope of the current explanation, it is worth noting that the quantum nature of spin simplifies the current problem. Unlike a classical rotating object, where angular momentum can be gained or lost through interactions with the surrounding environment, quantum spin is an intrinsic property of the particles under discussion and thus is a constant quantity. Thus, all protons have the same constant angular momentum and by extension the same constant magnetic moment:

$$\mu = \gamma L = \frac{\gamma \hbar}{2} \quad (1.5)$$

where  $\hbar$  is Planck’s constant. The macroscopic behaviour observed in NMR experiments is a result of the behaviour of a large number of nuclei. To translate these effects from an individual nucleus to a large collection of nuclei requires the use of Boltzmann statistics. According to Boltzmann statistics, the probability that a proton will be oriented at an angle  $\theta$  with an externally applied magnetic field  $P(\theta)$  is:

$$P(\theta) = \frac{\exp\left(-\frac{E_M(\theta)}{kT}\right)}{\int_0^\pi \exp\left(-\frac{E_M(\theta)}{kT}\right) \sin\theta \, d\theta} \quad (1.6)$$

where  $E_M(\theta)$  is the potential energy of a proton at angle  $\theta$  with the  $z$ -axis (see Equation 1.4),  $T$  is the temperature of the system in Kelvin, and  $k$  is Boltzmann's constant. From this, the average net magnetization along the  $z$ -axis from a single proton  $\langle\mu_z\rangle$  is:

$$\langle\mu_z\rangle = \int_0^\pi P(\theta) * \mu \cos\theta \sin\theta \, d\theta \approx \frac{\gamma^2 \hbar^2 B_0}{4kT} \quad (1.7)$$

If we have a sample composed of  $N$   $^1\text{H}$  nuclei, we can calculate the net magnetization for a sample ( $M_0$ ) by summing the contribution from each proton:

$$M_0 = N\langle\mu_z\rangle \approx \frac{\gamma^2 \hbar^2 N B_0}{4kT} \quad (1.8)$$

where  $N$  is the total number of nuclei in our system. From this, we can easily identify the experimental factors that affect the strength of the NMR effect; the number of  $^1\text{H}$  nuclei in the sample, sample temperature (measured in Kelvin), the strength of our applied magnetic field, and the gyromagnetic ratio of the nucleus being examined.

It is worth noting at this point that the behaviour derived above can be extended to other atomic nuclei beyond  $^1\text{H}$ . The mathematics involved are the same in principle, but are complicated by the presence of additional nucleons; as with the proton, the neutron also has quantum mechanical spin and generates its own dipole moment; these moments add to produce the magnetic moment of a more complex nucleus. Here the gyromagnetic ratio becomes an important factor; larger and more complex nuclei have a smaller charge to mass ratio. This results in a smaller gyromagnetic ratio, which in turn means a smaller  $M_0$  is generated for larger nuclei under constant experimental conditions. This fact, combined with the naturally high

abundance of  $^1\text{H}$  in biological systems has made hydrogen the primary nucleus of interest in medical applications of NMR.

### 1.3.3 Excitation

The utility of NMR comes from our ability to link the physical properties of the sample to the behaviour of sample magnetization. There is very little useful information that can be gleaned from simply measuring sample magnetization while it is statically aligned along the  $z$ -axis (often referred to in NMR as the longitudinal axis). However, if we can push sample magnetization away from equilibrium such that it has a component in the  $xy$ -plane (also known as the transverse plane), the natural precession of magnetization around  $B_0$  can be manipulated to reveal a wide range of useful information. Transverse magnetization is typically generated by applying a second, time varying magnetic field  $B_1(t)$  which oscillates sinusoidally with the same frequency as the precessing nuclei in our sample ( $\omega$ ), known as the Larmor frequency:

$$B_1(t) = |B_1(t)|\sin \omega t \quad (1.9)$$

This has the effect of rotating the entire distribution of magnetic moments away from the  $z$ -axis by an angle determined by the duration and amplitude of the pulse used.

In modern NMR techniques, pulsed  $B_1(t)$  fields, where the amplitude of  $B_1(t)$  is modulated over time, are almost universally used. The oscillatory frequency for this pulse as defined in Equation 1.9 falls into the radio frequency range for NMR experiments; as a result,  $B_1(t)$  is commonly referred to as a radiofrequency (RF) pulse. A given RF pulse will excite signal across a range of frequencies centered on the Larmor frequency. To take advantage of this, the amplitude modulation of  $B_1(t)$  in the time domain is

specifically tailored to give a desired frequency selection profile, while the duration of the pulse can be changed to give a desired frequency bandwidth.

### 1.3.4 Signal Detection

Detection of NMR signal relies on the principles of electromagnetic induction, which describes how a changing magnetic field generates electrical currents within a conductor:

$$\Phi_B = \int \mathbf{B}(\mathbf{r}, t) \cdot d\mathbf{A} \quad (1.10)$$

$$\epsilon = -\frac{d\Phi_B}{dt} \quad (1.11)$$

where  $\epsilon$  is the voltage generated,  $A$  is the area of the conductor where voltage is being induced, and  $\Phi_B$  is the magnetic flux through this area. In a simple NMR experiment, signal detection is achieved by placing a simple loop of wire adjacent to our sample with its cross sectional area parallel to  $\mathbf{B}_0$ . In this position, the precessing magnetization generates a sinusoidally varying voltage within the loop, which can then be measured as NMR signal. More complex NMR and MRI systems make use of more complicated conducting arrays that exploit this same principle, but are able to collect more detailed information over a region of interest.

### 1.3.5 Relaxation

Once magnetization has been pushed into the transverse plane, a variety of mechanisms will return it to equilibrium in a process known as relaxation. This process occurs exponentially, as described by Equations 1.12 and 1.13:

$$M_z(t) = M_0(1 - e^{-\frac{t}{T_1}}) \quad (1.12)$$

$$M_{XY}(t) = M_0 e^{-\frac{t}{T_2}} \quad (1.13)$$



where  $T_1$  is the relaxation constant which dictates how fast equilibrium magnetization is restored along the longitudinal axis,  $T_2$  is the relaxation constant which dictates how fast signal in the transverse plane disappears, and  $t$  is the time elapsed since excitation.

Relaxation is heavily dictated by the microenvironment experienced by individual magnetic moments within a sample. Molecular motion and the precession of neighbouring magnetic moments cause small fluctuations in the magnetic field seen by a given magnetic moment. In  $T_1$  relaxation, these local fluctuations cause precessing nuclei to lose energy to the surrounding environment. This energy loss only occurs when the fluctuations occur at or near the Larmor frequency. It is worth highlighting that  $T_1$  relaxation is effected by  $\mathbf{B}_0$  field strength. Equation 1.3 shows that the Larmor frequency depends on  $\mathbf{B}_0$ ; as  $\mathbf{B}_0$  increases, higher frequency fluctuations are required to return magnetization to the  $z$ -axis. As the frequency of molecular motion within our sample is constant with magnetic field, this increase in  $\mathbf{B}_0$  lengthens  $T_1$  relaxation by increasing the frequency separation between molecular motion and resonance frequency.

$T_2$  relaxation is caused by similar mechanisms, but crucially in  $T_2$  relaxation energy is simply exchanged between moments within a sample and there is no net energy loss to the surrounding environment. When signal is excited in an NMR experiment, transverse relaxation is created by the coherent precession of nuclei around  $\mathbf{B}_0$ . Fluctuations in the field seen by each nucleus causes variations in precession frequency, leading to a loss of coherence and hence a loss in transverse magnetization over time. This loss of coherence largely results from low frequency magnetic fluctuations; these effects are amplified as we move to very high field strengths, leading to shorter  $T_2$  relaxation times.

Up to now we have assumed that the applied  $B_0$  is an ideal, completely uniform field. In reality this field is generated over a finite region and hence is heterogeneous to some degree across a sample. In addition, the sample has an effect on  $B_0$ ; different materials have different magnetic properties, and when there is a transition between different materials within a magnetic field (such as the transition between a sample and the surrounding air) fluctuations in  $B_0$  occur. Modern MRI systems come equipped with hardware known as shimming coils that are used correct for gross inhomogeneities in  $B_0$ ; however, small variations are omnipresent in any real NMR experiment. These non-idealities are important from a relaxation standpoint as they can dramatically speed up transverse relaxation. For a given magnetic moment, the resonance frequency depends on the total local magnetic field encountered by that moment; generalizing Equation 1.3, we find:

$$\omega = \gamma B = \gamma(B_0 + \Delta B) \quad (1.14)$$

where  $\Delta B$  represents any variation in  $B_0$  due to magnetic inhomogeneities, applied  $B_1$  fields, or applied magnetic gradients (discussed below).

These shifts in the resonance frequency across the sample due to  $B_0$  inhomogeneities causes our magnetization to dephase much more rapidly than theoretical  $T_2$  decay. However, because these inhomogeneities are constant in time and space their effect can be reversed using by RF pulses to invert phase. For this reason, the simple observed transverse relaxation in a given experiment is referred to as  $T_2^*$  decay, and we reserve the term  $T_2$  relaxation for the irreversible decay previously described (Figure 1.5).

### 1.3.6 Gradients

The most powerful tool available to link the physical properties of a sample to its magnetization is the magnetic gradient. By applying a linearly varying magnetic gradient across a sample, we can linearly vary the resonance

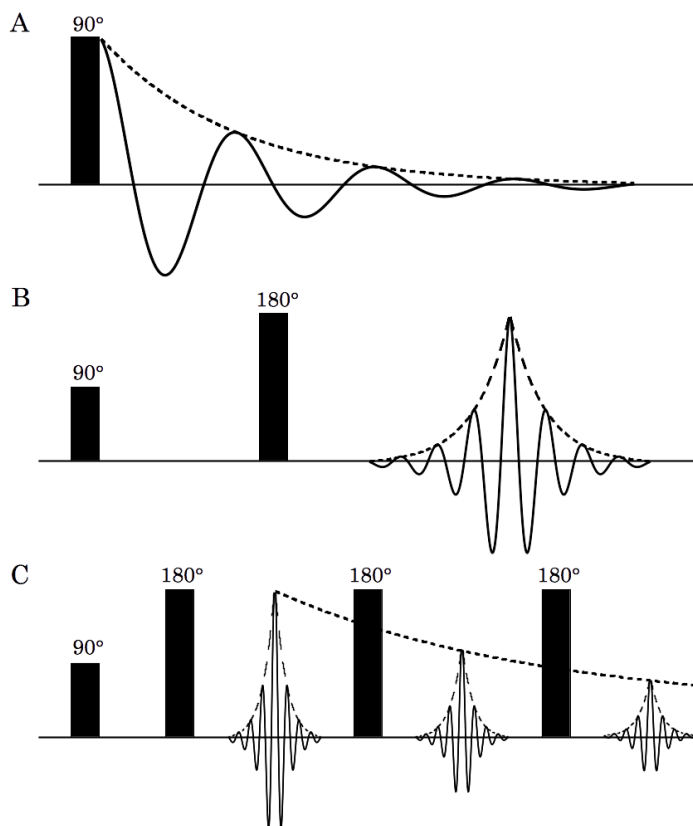


**Figure 1.5 - Simple Pulse Sequences Illustrating Relaxation Effects:** (A) shows a Free Induction Decay where signal decays exponentially at the rate  $T_2^*$  (dotted line). (B) shows a Spin Echo where the echo rises and falls exponentially according to  $T_2^*$ . (C) shows a Carr-Purcell-Meiboom-Gill (CPMG) echo train, which uses a series of 180 degree RF pulses to refocus an echo multiple times. Here the maximum amplitude of each echo decreases exponentially at the rate  $T_2$ .

frequency of nuclei across our sample in a highly controlled manner (see Equation 1.14). This creates a spatial dependence between signal phase and position that has two main uses.

When applied in conjunction with an RF pulse, an applied magnetic gradient can excite signal from a slab or slice of the sample, and is known as a slice select gradient. As mentioned above, RF pulses excite signal from any precessing moments that fall within a certain frequency range around the Larmor frequency. By varying the strength of a magnetic gradient, signal from specific slices of the sample can be excited and acquired, allowing for localized NMR measurements within a large or heterogeneous sample. Gradients are also fundamental for producing images. The relationship created between resonance frequency and position created by magnetic gradients can be exploited to produce dependence between the position of a magnetic moment within the MR system and its phase. Stated simply, the inverse Fourier transform of an NMR signal acquired in the presence of a magnetic field gradient returns the frequency distribution of the signal induced by the gradient, which can be used to recover the spatial distribution of magnetization, producing an image of the sample.

### **1.3.7 Magnetic Resonance Spectroscopy**

Magnetic resonance spectroscopy (MRS) is a technique that allows for the identification and quantification of different chemical species within a sample.

#### **1.3.7.1 Chemical Shift**

Prior to this discussion, we have been tacitly assuming that our hypothetical sample was composed exclusively of  $^1\text{H}$  nuclei. In reality, this picture is complicated by the presence of chemical structure within a sample and the electrons that form these structures. As with protons and neutrons, electrons

generate their own magnetic dipole that causes a slight local variation in  $B_0$ . This causes a shift in the resonance frequency between  $^1\text{H}$  nuclei attached to different molecules, and between chemically non-equivalent  $^1\text{H}$  nuclei within the same molecule. These variations from the Larmor frequency occur by a fixed percentage (usually measured in parts-per-million, ppm) and are heavily dependent on the chemical structure of the molecule. Magnetic resonance spectroscopy exploits this behaviour to identify different chemical species. Using the Fourier transform, a time-domain signal collected from an NMR system is decomposed into its frequency components, allowing us to visualize the resonance frequencies present within a sample. Using either computer simulations or phantom measurements of a single molecule of interest in isolation, the characteristic pattern of frequency shifts, peak amplitudes, and phases can be modeled for that molecule of interest. This information is then used to identify that molecule from a more complicated spectrum composed of many molecules (Figure 1.6).

The signal amplitude in NMR is proportional to the number of nuclei generating that signal. Following a Fourier transform, this relationship results in the number of nuclei involved instead being proportional to the area under the corresponding spectral peak. This allows the concentration of chemicals to be measured quantitatively by comparing the area under the spectral peaks of different molecules to a reference signal with known concentration.

### 1.3.7.2 J-coupling

While chemical shift is primarily responsible for MRS phenomena, these spectra are further shaped by the phenomenon of J-coupling. To explain J-coupling we must briefly invoke quantum mechanics. In quantum mechanics there is a principle known as Pauli's exclusion principle. This rule simply states that particles with half integer spin cannot occupy the same quantum

state within the same system simultaneously (i.e. different particles within a system must be distinct). Protons, neutrons, and electrons all have half integer spin and hence all follow this rule. However, for our purposes this principle is most important for the electron.

When bound to an atom or molecule, electrons are confined by quantum mechanics to a discrete set of orbitals surrounding their parent nuclei; each orbital can contain up to two electrons. Electrons within the same orbital by definition share many quantum properties, leaving quantum spin ( $m$ ) as the only variable that can be used to distinguish between them. As a result, for pairs of electrons within the same orbital, one electron must be in a spin down state ( $m = \frac{1}{2}$ ), and the other must be in a spin up state ( $m = -\frac{1}{2}$ ).

When applied to the electrons that bind a molecule together, the exclusion principle provides a mechanism for nuclei to affect the chemical shift of other nuclei they are chemically bonded to. The polarization of one nucleus along the  $z$ -axis in a molecule will affect the polarization of its accompanying electrons. This restricts the polarization of electrons from other nuclei that share orbitals connecting the first nucleus to a second, thus subtly affecting the chemical shift of this second nucleus. This effect is not simply restricted to adjacent nuclei, but can alter the signal from chemically distinct nuclei up to 3 chemical bonds away from one another.

In an MR spectrum, this effect causes spectral peaks to be split into multiple daughter peaks (Figure 1.7). This information can be useful because it contains information about the structure of the molecule. However, depending on the strength of the coupling, this can lead to a substantial decrease in the signal to noise ratio (SNR) of a spectrum, and cause significant overlap between signals from different molecules, increasing measurement difficulty.

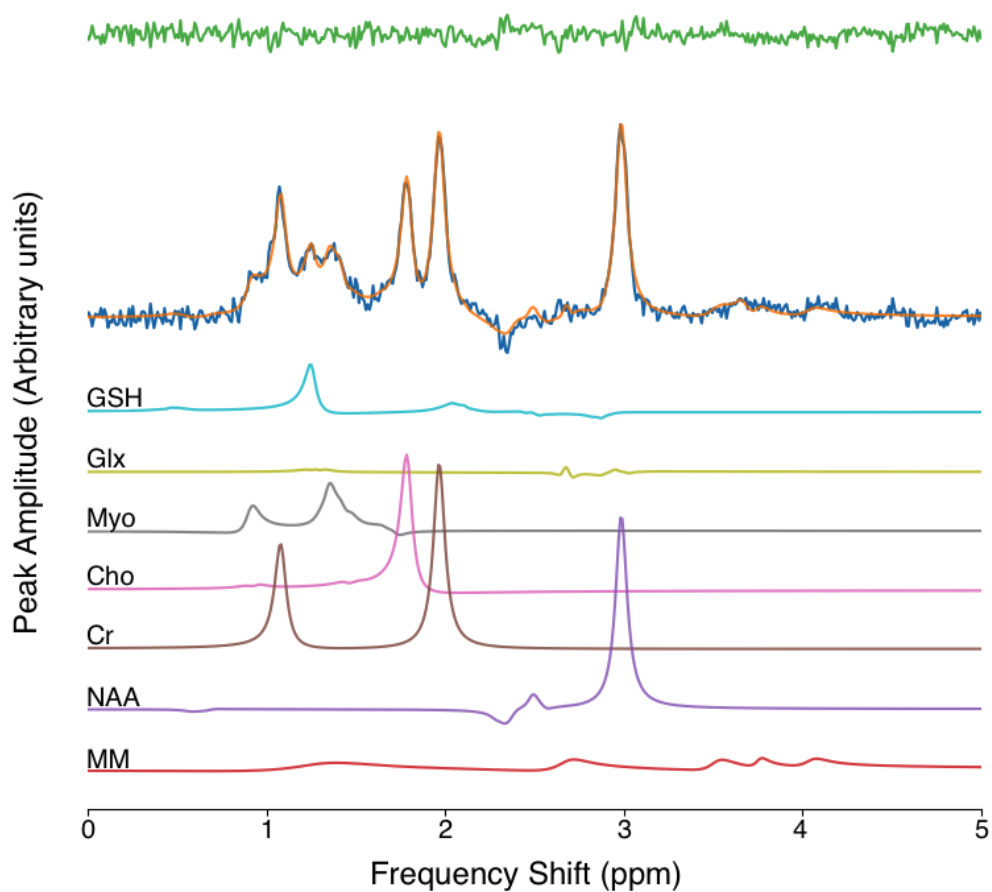


**Figure 1.6 – Fit 7T semi-LASER Spectrum Collected from the Hippocampus:** Spectrum collected from a human hippocampus (blue), overlaid with fit spectrum (orange) and residual noise (green). Below, the fit spectrum is broken down into the contributions from individual metabolites. Data was acquired using a semi-LASER sequence (See section 1.3.7.6)

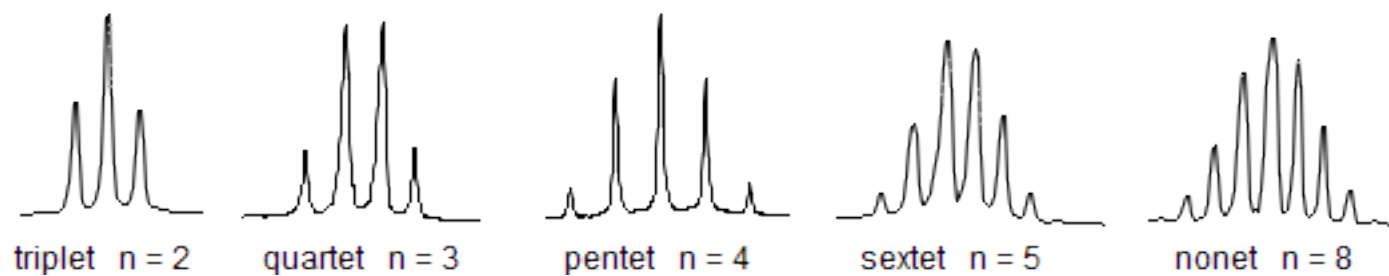


**Figure 1.7 - Example J-coupling Multiplets:** Example multiplets from NMR experiments; if J-coupling were not a factor, all these multiplets would stack on top of one another to create a single, high amplitude peak.

Multiplet image by ChemistHans at English Wikipedia [Public domain], via Wikimedia Commons



### 1.3.7.3 Spectroscopic Techniques

To collect a spectrum one simply has to excite nuclei within the sample, then record and Fourier transform the resulting signal waveform. However, particularly for medical applications, spatial localization of spectroscopic signal is necessary to identify metabolic change in abnormal, diseased, or damaged tissue. As a result, a variety of techniques have been developed to encode spatial information. The simplest forms of localized spectroscopic techniques are known as single voxel techniques; these techniques collect bulk signal from a specific region of interest. In all single voxel techniques, three slice selective gradients applied across the  $x$ -,  $y$ -, and  $z$ -axes are used to selectively excite signal from the region of interest. For a more detailed view of a region of interest, magnetic resonance spectroscopic imaging (MRSI) can be used. This technique involves collecting spectra from voxels arranged in a grid pattern across a region of interest to generate maps of different metabolite levels across that region.

The key limitation on the use of spectroscopic techniques in medical practice is the low concentration of most metabolites *in vivo*. As shown in Equation 1.8, sample magnetization (and hence sample signal) is proportional to the number of relevant nuclei being excited. While water is highly concentrated in tissue (with an average concentration of  $\sim 50$  M in the human brain), many of the metabolites of interest in *in vivo* NMR have relatively low concentrations on the order of mM. This has two effects; first, to accurately quantify metabolite signal, water suppression techniques must be employed to prevent water signal from completely overwhelming the rest of a spectrum. Second, the low metabolite signal results in a low SNR for these spectral peaks. To accurately quantify metabolite levels, signal averaging is often necessary to boost SNR, which results in long scan times that are not ideal in

a clinical environment. This is particularly true for MRSI techniques that require the collection of multiple spectra across a sample.

#### **1.3.7.4 Data Analysis Methods and Techniques**

In MRS, the exact data analysis steps taken to convert from an MRS spectrum to a measure of concentration varies between different research groups. Discussed here will be the analysis techniques used for the research presented in Chapter 2.

Prior to analysis, spectral data typically undergo some pre-processing to improve spectral quality. Time and spatially varying field inhomogeneities may distort the shape of the peaks within a spectrum, making the quantification process more difficult. To reduce this effect, various lineshape corrections are possible. In this study presented in Chapter 2, we utilized a combined QUALITY deconvolution [32] and eddy current correction [33] (QUECC) technique to ensure spectral peaks all had a Lorentzian lineshape [34].

Metabolite concentration is calculated from an MRS spectrum based on the relationship between the number of nuclei generating a signal and the signal amplitude. By measuring the amplitude associated with each metabolite in the time domain, concentration can be calculated. This amplitude is measured by fitting a simulated metabolite prior knowledge lineshapes, generated using the PyGamma pulse sequence simulation tools [35], to the acquired data. A Levenberg-Marquard minimization routine is used to minimize the difference between the data and the prior knowledge lineshapes. The model is constrained in how it can fit the data to ensure errors do not occur; for example, if the fit for a specific spectral peak falls outside of the given constraints, then that peak's time domain amplitude is fixed to zero and fitting is re-started. Once the data is accurately fit, the

signal amplitudes of each metabolite determined from the fit are used to calculate concentrations [36], [37].

Concentration is commonly calculated in the brain either as absolute values in mM using water as an internal reference signal, or as a ratio to the molecule creatine (Cr). Ratios to creatine were calculated by summing the peak amplitudes that contribute to a particular metabolite spectrum, then dividing by the total amplitude of Cr (Equation 1.15):

$$X/Cr = \frac{\Sigma S_{Amp,X}}{\Sigma S_{Amp,Cr}} \quad (1.15)$$

where  $X/Cr$  is the concentration of the metabolite of interest  $X$  as a ratio to Cr, and  $\Sigma S_{Amp,X}$  and  $\Sigma S_{Amp,Cr}$  are the total amplitude of all peaks that form the spectral line shape of the metabolite of interest and Cr.

Absolute concentration calculations, which give metabolite concentration within the combined grey/white matter tissue fraction of the voxel, were evaluated using Equation 1.16:

$$[X]_{Tissue} = \frac{\Sigma S_{Amp,X}}{\Sigma S_{Amp,H_2O}} \frac{n_{\rho,H_2O}}{n_{\rho,X}} \frac{R_{H_2O}}{R_X} * [H_2O]_{Voxel} * (GM + WM) \quad (1.16)$$

$$R_X = GM \left( 1 - e^{-\frac{TR}{T_{1,GM}}} \right) \left( e^{-\frac{TE}{T_{2,GM}}} \right) + WM \left( 1 - e^{-\frac{TR}{T_{1,WM}}} \right) \left( e^{-\frac{TE}{T_{2,WM}}} \right) \quad (1.17)$$

Where  $[X]_{Tissue}$  is the concentration of the metabolite of interest within the tissue fraction of the MRS voxel,  $n_{\rho,H_2O}$  and  $n_{\rho,X}$  are the number of protons producing spectral signal for both water and the metabolite of interest,  $R_X$  and  $R_{H_2O}$  are the combined  $T_1$  and  $T_2$  relaxation for both the metabolite of interest and water in grey and white matter (See Equation 1.17),  $[H_2O]_{Voxel}$  is the average concentration of water within the voxel, and  $(GM+WM)$  is the

voxel tissue fraction for grey and white matter [38]. This last correction was included to ensure that the calculated metabolite concentration was the average concentration within the tissue component of the voxel, and not from the voxel as a whole. For this calculation, voxel tissue volume fractions were evaluated using the Oxford Centre for Functional MRI of the Brain (FMRIB) software library (FSL) [39]; images were brain extracted and segmented using FSL's Brain Extraction Tool (BET) [40] and FMRIB's Automated Segmentation Tool (FAST) [41]. Literature reported relaxation and water concentration values were used for this calculation [42]–[45].

### 1.3.7.5 Effects of Field Strength in Spectroscopy

As previously mentioned, the low concentration of metabolites *in vivo* results in a low SNR in MRS measurements, which in turn decrease the clinical utility of MRS by requiring long scan times. Looking back to Equation 1.8, the only factor that can be manipulated to increase SNR for an *in vivo* measurement is  $B_0$ . In addition, as mentioned in the discussion of chemical shift, the shift between different spectral peaks is a fractional change away from the Larmor frequency. By increasing  $B_0$ , the frequency separation between different spectral peaks increases (spectral dispersion), making it easier to separate overlapping peaks, allowing for the independent measurement of metabolites that are heavily overlapped at lower field strengths. For these two reasons, MRS can greatly benefit from an increase in  $B_0$  field strength, leading to a push to perform MRS on the strongest possible magnets.

However, while an increase in  $B_0$  had considerable benefits, it also increases magnetic field inhomogeneities in biological tissues. MRS relies on the resolution of frequency shifts to identify different molecules. However, frequency shifts can also be caused by variations in  $B_0$  within a region of study. With  $B_0$  variation, spectral peaks become wider and the SNR of a

collected spectrum decreases, potentially countering the benefits of higher field strength. Importantly, magnetic susceptibility artefacts increase with  $B_0$ . At ultra-high field strengths ( $\geq 7\text{T}$ ), these non-uniformities must be corrected using a combination shimming hardware and inhomogeneity insensitive MRS pulse sequences to preserve the benefits of increased field strength. In addition, the increase in Larmor frequency requires higher energy  $B_1$  fields, which are in turn harder to generate uniformly across a sample, and can lead to power deposition restrictions.

An additional source of error in MRS localization that increases with field strength is the chemical shift displacement error (CSDE). Spatial localization is achieved for MRS primarily through frequency selective excitation; a gradient is applied across a sample, then an RF pulse excites signal from a specific range of frequencies that correspond to the region of interest.

However, in MRS the excited signal contains substantial contributions from metabolite peaks that are not oscillating at the Larmor frequency prior to gradient application. This means that the signal from each spectral peak comes from a slightly different voxel, with a displacement given by Equation 1.18:

$$\Delta x = \frac{\Delta\omega}{\Delta\omega_{max}} V_x \quad (1.18)$$

where  $\Delta x$  is the change in position for the centre of the voxel along the  $x$ -axis,  $\Delta\omega$  is the chemical shift between two spectral peaks,  $\Delta\omega_{max}$  is the bandwidth of the slice selective RF pulse, and  $V_x$  is the voxel length along the  $x$ -axis. To minimize CSDE either high powered gradients, or high bandwidth RF pulses must be used during slice selection [30].

### 1.3.7.6 Semi-LASER

Localization by adiabatic selective refocusing (LASER) [46] is a spectroscopy localization sequence designed to acquire high quality MRS spectra from well defined voxels at ultra-high field strengths. A slight variant of this sequence called semi-LASER uses a simple, slice selective sinc shaped  $90^\circ$  RF pulse to excite signal, followed by two pairs of slice selective adiabatic full passage (AFP) pulses to localize signal to a single voxel of user specified dimensions (Figure 1.8). The sequence produces a spin echo; the second half of the echo is acquired and Fourier transformed to produce the MRS spectrum.

Adiabatic pulses are a class of RF pulse that are both modulated in amplitude and frequency over the duration of the pulse. These pulses are designed to be less sensitive to  $B_1$  inhomogeneities than conventional pulses, and therefore particularly useful for high field applications where  $B_1$  may vary across a sample. In addition, adiabatic pulses can be designed to have large excitation bandwidths with arbitrarily long pulse durations. This has several advantages; for example, increasing pulse length allows for a decrease in pulse amplitude, which in turn reduces power deposition. Furthermore, high bandwidth pulses reduce chemical shift artefacts [30], [47], [48].

There are also drawbacks associated with adiabatic pulses; for example, they take a long time to play out, resulting in long echo times that reduce SNR. Also, when used for slice selection, proper refocusing can only be achieved by using paired adiabatic pulses. This increases the total number of pulses and increases overall power deposition. The semi-LASER sequence is designed as a happy middle ground between more conventional single voxel techniques and LASER. In semi-LASER, localization is achieved using two slice selective AFP pulse pairs and a slice selective normal RF pulse at the beginning of the

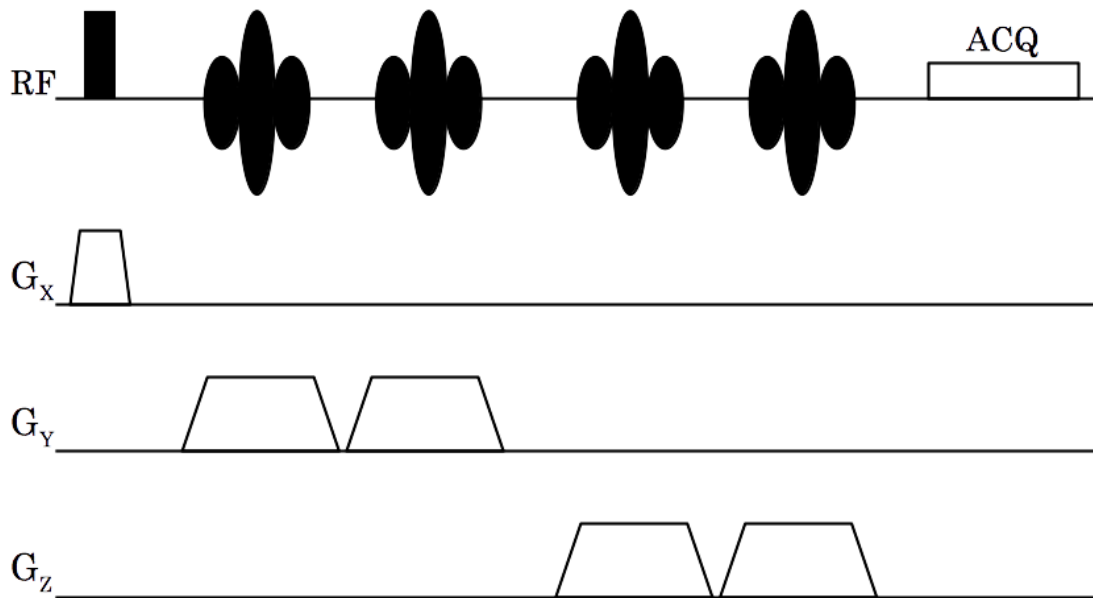


**Figure 1.8 - The semi-LASER Pulse Sequence:** In this sequence, initial excitation is performed with a  $90^\circ$  sinc shaped slice select pulse. This is followed by two pairs of slice select adiabatic full passage pulses, which localize signal to a voxel within the sample while refocusing signal into a spin echo. The decay of this echo is then acquired and Fourier transformed to give an MRS spectrum

sequence, creating a balance between reduced echo time and power transmission [30], [47], [48].

## 1.4 Spectroscopy in Temporal Lobe Epilepsy

MRS was first applied to the study of human epilepsy in the late 1980's, with TLE being one of the first epilepsies examined [49]. In the decades since, dozens of research groups have examined TLE with MRS, the results of which are summarized below based on the metabolite of interest.

### 1.4.1 Creatine

Biologically, Cr acts as a buffer for cellular energy metabolism. Cr exists in two main forms in the human body; molecular creatine, and phosphocreatine (PCr). The enzyme creatine kinase can rapidly convert between these two molecules via the following reaction:



turning adenosine triphosphate (ATP) into adenosine diphosphate (ADP) or vice versa in the process. ATP is the primary energy-carrying molecule in cellular processes; by storing high-energy phosphorus bonds in PCr, the cell creates an energy reservoir that can be used to rapidly replenish ATP levels in response to increased energy consumption. Furthermore, PCr is able to diffuse much faster throughout a cell than ATP, allowing for more efficient energy transport. In *in vivo* MRS studies, the signal from both forms of Cr overlap significantly with one another in the spectrum. As a result, Cr concentration is commonly measured as the total concentration of these two molecules [30], [50].

Creatine is particularly noteworthy in MRS studies of the brain in general because its concentration *in vivo* has been shown to be invariant with age



and invariant between healthy and diseased tissue in some diseases. This suggests that Cr is a good candidate as a reference signal with which to quantify other metabolites. As a result, many MRS studies report metabolite concentration as a ratio of the metabolite of interest to Cr (denoted as X/Cr). However, more recent work has shown that Cr is not constant between healthy and diseased tissue under a variety of conditions, making its use as a reference signal a potential source of error [30], [50]. Some argue that the potential variance in concentration undermines the accuracy of MRS measurements [50], whereas others have commented that normalization to creatine still gives a useful measurement, as it potentially normalizes for the amount of biomass within a measured region [51].

In epilepsy, due to its common use as a reference signal, few studies report on the behaviour of Cr directly. In one study [9], Cr levels (measured as an absolute quantity using an internal water reference, hereafter denoted by enclosing metabolite shorthand within [square brackets]) were found to increase ipsilateral to seizure focus in patients with drug-resistant mesial temporal sclerosis. Meanwhile other studies did not observe changes in [Cr] in TLE patients with hippocampal sclerosis or in MRI-negative TLE patients [52], [53]. In another study [54], high resolution scans of resected epileptic tissue found that elevated [Cr] levels were associated with elevated seizure frequency, but were not different between samples with hippocampal sclerosis compared to samples with no visible lesion.

#### 1.4.2 *N*-Acetylaspartate

*N*-Acetylaspartate (NAA) is one of the most highly concentrated metabolites within the brain; this in combination with its very prominent methyl singlet peak at 2.01 ppm makes it the easiest metabolite to measure in an *in vivo* spectrum. It is exclusively synthesized in neuronal mitochondria, making it a biomarker for neuronal health and density. NAA levels have been found to

decrease across a wide range of neurological disorders, and have been found to recover in some diseases in response to treatment [30], [50].

In TLE, decreased NAA levels ipsilateral to seizure focus are the most commonly reported metabolic changes, both when measured as the ratio NAA/Cr [55], [56] or NAA/(Cr+ Cho) [57]–[60], and as an absolute quantity [9], [52]. Studies have also found that NAA change is not limited to the epileptic focus; decreases in NAA have been reported outside of visible lesions ipsilateral to seizure focus [56], contralateral to seizure focus [55], and various regions of the frontal lobe [61], [62]. Using an MRSI technique, one study [63] showed that when the area of greatest NAA/Cr abnormality was resected, patients had better clinical outcomes. In MRI-normal TLE patients, changes in NAA appear to be less distinct. Some report the same NAA decrease as that seen in lesional TLE [64], while others report no difference between MRI-normal patients and healthy controls [52]. NAA levels may also be affected by seizure activity, as one study has found decreases in NAA/Cr, NAA/Cho, and NAA/(Cr+ Cho) when comparing patients immediately post seizure to their inter-ictal baseline [65].

### 1.4.3 Choline

The choline (Cho) signal in NMR is the product of signal from a variety of choline containing molecules, namely free choline, phosphocholine, and glycerophosphocholine. These 3 molecules are all involved in the process of phospholipid synthesis and degeneration, and as a result changes in Cho in MRS are largely associated with membrane turnover. It is also important to note that Cho is readily transported across the blood brain barrier, as the brain does not synthesize enough to meet its needs. As a result, Cho levels in the brain can be affected by diet. Cho is the second most prominent peak from human brain spectra, because it contains 9 chemically equivalent protons

that do not experience substantial chemical shift effects between different Cho containing metabolites [30], [50].

In TLE, Cho is commonly included into the combined measure NAA/(Cho+Cr) or NAA/Cho, both of which have been shown to decrease ipsilateral to seizure focus [56], [57], [60], [62], [65]. In cases Cho is reported, it has been found to increase ipsilateral to seizure focus [9] or has shown no significant change [66]. In resected tissue, [Cho] was found to be lower in lesional TLE tissue compared to MRI-normal tissue [54].

#### 1.4.4 Glutamate and Glutamine

Glutamate (Glu) is the highest concentration amino acid in the central nervous system. However, unlike NAA or Cho none of the 5 protons on the Glu molecule are chemically equivalent. As a result, the Glu spectrum is split into a large number of low amplitude peaks. Furthermore glutamine (Gln), the precursor molecule for Glu, is structurally very similar to glutamate; this results in a high level of overlap between the spectra for these two molecules making them very hard to resolve independently at clinical field strengths. As a result, for *in vivo* studies they are almost always reported as a combined concentration (Glx).

Biologically, glutamate is important because it is the primary excitatory neurotransmitter in the CNS. Importantly for epilepsy, Glu can also be neurotoxic. One of the receptors Glu activates allows positively charged  $\text{Ca}^{2+}$  ions into a neuron, which in sufficient quantities can cause cell death. Meanwhile, glutamine is a molecule that is synthesized from Glu in astrocytes. After a neuron releases Glu during neurotransmission, that Glu is taken out of the synaptic cleft by astrocytes. It is then converted from Glu to Gln so it can be safely transferred back to the neuron for re-synthesis of Glu

in what is known as the Glu-Gln cycle. In addition, Gln is used to synthesize the primary inhibitory neurotransmitter, GABA [30], [50].

In epilepsy, dysfunction of the Glu-Gln cycle is considered one of the potential causes of seizures, making Glx studies a key area of interest [8]. In TLE, the region of the brain involved further complicates evaluation of Glx.

Specifically, the proximity of the temporal lobe to the base of the skull and sinuses results in increased  $B_0$  heterogeneity. This decreases the SNR of the spectrum and makes it challenging to separate Glx signal from noise at clinical field strengths. Of the studies that do report Glx levels, two did not find significant changes [66], [55], one found Glx/Cr decreased ipsilateral to seizure focus compared to controls and contralateral tissue [58], one found a significant increase in [Glu] and [Gln] in lesional TLE tissue compared to MR normal tissue [54], and one found that Glu increased in the frontal lobe of TLE patients [52].

#### 1.4.5 *Myo-Inositol*

*Myo*-inositol (*Myo*) is the most prevalent form of inositol in the human body. Within the CNS, *Myo* is understood to take on several roles; it is part of the lipid component of biological membranes, it is an osmolyte used to maintain cell volume, and it both acts as and is used to synthesize secondary messenger molecules for intra-cellular communication. As with Cho, *Myo* is transported across the blood brain barrier and is primarily sourced both from synthesis elsewhere in the body and from dietary supplementation. In MRS, *Myo* has been proposed as a biomarker for glial cell activity. However, *Myo* has been shown to be taken up by neurons as well as glial cells, leading to questions about its specificity [30], [50].

In the study of TLE, levels of *Myo*/Cr have been reported to decrease ipsilateral to seizure focus in MRI-normal TLE patients [58], to increase

ipsilateral to seizure focus in patients with hippocampal sclerosis [52], and to decrease in frontal lobe in TLE patients [52], [61].

## **1.5 Thesis Outline**

To address our research question outlined in Section 1.1, we performed an MRS study of non-lesional TLE patients to identify metabolic abnormalities associated with this patient group. This study and its results are detailed in Chapter 2. The final chapter contains a brief overview of our results thus far, and the future direction in which this work could be taken.

## References

- [1] R. S. Fisher *et al.*, “Epileptic seizures and epilepsy: Definitions proposed by the International League Against Epilepsy (ILAE) and the International Bureau for Epilepsy (IBE),” *Epilepsia*, vol. 46, no. 4, pp. 470–472, 2005.
- [2] A. W. C. Yuen, M. R. Keezer, and J. W. Sander, “Epilepsy is a neurological and a systemic disorder,” *Epilepsy Behav.*, vol. 78, pp. 57–61, 2018.
- [3] W. F. Peng *et al.*, “Increased ratio of glutamate/glutamine to creatine in the right hippocampus contributes to depressive symptoms in patients with epilepsy,” *Epilepsy Behav.*, vol. 29, no. 1, pp. 144–149, 2013.
- [4] L. Nashef, E. L. So, P. Ryvlin, and T. Tomson, “Unifying the definitions of sudden unexpected death in epilepsy,” *Epilepsia*, vol. 53, no. 2, pp. 227–233, 2012.
- [5] J. P. Betjemann and D. H. Lowenstein, “Status epilepticus in adults,” *Lancet Neurol.*, vol. 14, no. 6, pp. 615–624, 2015.
- [6] J. J. Falco-Walter, I. E. Scheffer, and R. S. Fisher, “The new definition and classification of seizures and epilepsy,” *Epilepsy Res.*, vol. 139, no. July 2017, pp. 73–79, 2018.
- [7] W. Muhlhofer, Y. L. Tan, S. G. Mueller, and R. Knowlton, “MRI-negative temporal lobe epilepsy—What do we know?,” *Epilepsia*, vol. 58, no. 5, pp. 727–742, 2017.
- [8] F. Al Sufiani and L. C. Ang, “Neuropathology of Temporal Lobe Epilepsy,” *Epilepsy Res. Treat.*, vol. 2012, pp. 1–13, 2012.
- [9] K. N. Fountas, I. Tsougos, E. D. Gotsis, S. Giannakodimos, J. R. Smith, and E. Z. Kapsalaki, “Temporal pole proton preoperative magnetic resonance spectroscopy in patients undergoing surgery for mesial temporal sclerosis,” *Neurosurg. Focus*, vol. 32, no. 3, p. E3, 2012.
- [10] M. F. Bear, B. W. Connors, and M. A. Paradiso, *Neuroscience: Exploring*

- the Brain*, 4th ed. Wolters Kluwer, 2016.
- [11] C. E. Stafstrom and L. Carmant, “Seizures and Epilepsy : an overview for neuroscientist,” *Cold Spring Harb. Perspect. Med.*, vol. 5.6, p. a022426, 2015.
- [12] J. I. Sirven, “Epilepsy: A spectrum disorder,” *Cold Spring Harb. Perspect. Biol.*, vol. 7, no. 9, pp. 1–16, 2015.
- [13] H. Gray and W. H. Lewis, *Anatomy of the Human Body*, 20th ed. Lea & Febiger, 1918.
- [14] J. Sobotta, *Atlas and Textbook of Human Anatomy, Vol. 3*. Philadelphia: W.B. Saunders Company, 1908.
- [15] K. Ganesan and M. Ursekar, “Clinical utility of BOLD fMRI in preoperative work-up of epilepsy,” *Indian J. Radiol. Imaging*, vol. 24, no. 1, p. 22, 2014.
- [16] B. D. Clark, E. M. Goldberg, and B. Rudy, “Electrogenic tuning of the axon initial segment,” *Neuroscientist*, vol. 15, no. 6, pp. 651–668, 2009.
- [17] R. Khazipov, “GABAergic synchronization in epilepsy,” *Cold Spring Harb. Perspect. Med.*, vol. 6, no. 2, pp. 1–13, 2016.
- [18] M. Barker-Haliski and H. Steve White, “Glutamatergic mechanisms associated with seizures and epilepsy,” *Cold Spring Harb. Perspect. Med.*, vol. 5, 2015.
- [19] D. A. Coulter and C. Steinhäuser, “Role of astrocytes in epilepsy,” *Cold Spring Harb. Perspect. Med.*, vol. 5, 2015.
- [20] D. I. Kaplan, L. L. Isom, and S. Petrou, “Role of sodium channels in epilepsy,” *Cold Spring Harb. Perspect. Med.*, vol. 6, no. 6, p. a022814, 2016.
- [21] R. Köhling and J. Wolfart, “Potassium channels in epilepsy,” *Cold Spring Harb. Perspect. Med.*, vol. 6, no. 5, p. 24, 2016.
- [22] S. Rajakulendran and M. G. Hanna, “The role of calcium channels in epilepsy,” *Cold Spring Harb. Perspect. Med.*, vol. 6, no. 1, pp. 173–194, 2016.

- [23] A. Pitkänen, K. Lukasiuk, F. Edward Dudek, and K. J. Staley, “Epileptogenesis,” *Cold Spring Harb. Perspect. Med.*, vol. 5, no. 10, pp. 1–17, 2015.
- [24] M. O. Krucoff *et al.*, “Rates and predictors of success and failure in repeat epilepsy surgery: A meta-analysis and systematic review,” *Epilepsia*, vol. 58, no. 12, pp. 2133–2142, 2017.
- [25] F. J. López González *et al.*, “Drug-resistant epilepsy: Definition and treatment alternatives,” *Neurol. (English Ed.)*, vol. 30, no. 7, pp. 439–446, 2015.
- [26] W. O. Tatum *et al.*, “Clinical utility of EEG in diagnosing and monitoring epilepsy in adults,” *Clin. Neurophysiol.*, vol. 129, no. 5, pp. 1056–1082, 2018.
- [27] F. Cendes, “Neuroimaging in investigation of patients with epilepsy,” *Continuum (Minneap. Minn.)*, vol. 19, pp. 623–42, 2013.
- [28] J. S. Duncan, “Imaging and epilepsy,” *Brain*, vol. 120, no. 2, pp. 339–377, 1997.
- [29] D. G. Nishimura, *Principles of Magnetic Resonance Imaging*. Stanford: Stanford University, 2010.
- [30] R. A. DeGraaf, *in vivo NMR Spectroscopy*, 2nd ed. John Wiley & Sons, Ltd, 2007.
- [31] L. G. Hanson, “Is Quantum Mechanics Necessary for Understanding Magnetic Resonance,” *Concepts Magn. Reson. Part A*, vol. 32A, no. 5, pp. 329–340, 2008.
- [32] A. A. De Graaf, J. E. Van Dijk, and W. M. M. . Bovee, “QUALITY: Quantification Improvement by Converting Lineshapes to the Lorentzian type,” *Magn. Reson. Med.*, vol. 13, no. 3, pp. 343–357, 1990.
- [33] U. Klose, “In vivo proton spectroscopy in presence of eddy currents,” *Magn. Reson. Med.*, vol. 14, no. 1, pp. 26–30, 1990.
- [34] R. Bartha, D. J. Drost, R. S. Menon, and P. C. Williamson, “Spectroscopic lineshape correction by QUECC: Combined QUALITY



- deconvolution and eddy current correction,” *Magn. Reson. Med.*, vol. 44, no. 4, pp. 641–645, 2000.
- [35] S. a. Smith, T. O. Levante, B. H. Meier, and R. R. Ernst, “Computer Simulations in Magnetic Resonance. An Object-Oriented Programming Approach,” *J. Magn. Reson., Ser. A*, vol. 106, no. 1, pp. 75–105, 1994.
- [36] J. Penner and R. Bartha, “Semi-LASER <sup>1</sup> H MR spectroscopy at 7 Tesla in human brain: Metabolite quantification incorporating subject-specific macromolecule removal,” *Magn. Reson. Med.*, vol. 74, no. 1, pp. 4–12, 2015.
- [37] R. Bartha, D. J. Drost, and P. C. Williamson, “Factors affecting the quantification of short echo in-vivo <sup>1</sup> H MR spectra : prior knowledge , peak elimination , and filtering,” pp. 205–216, 1999.
- [38] R. Rupasingh, M. Borrie, M. Smith, J. L. Wells, and R. Bartha, “Reduced hippocampal glutamate in Alzheimer disease,” *Neurobiol. Aging*, vol. 32, no. 5, pp. 802–810, 2011.
- [39] M. Jenkinson, C. F. Beckmann, T. E. J. Behrens, M. W. Woolrich, and S. M. Smith, “Fsl,” *Neuroimage*, vol. 62, no. 2, pp. 782–790, 2012.
- [40] Y. Zhang, M. Brady, and S. Smith, “Segmentation of brain MR images through a hidden Markov random field model and the expectation-maximization algorithm,” *IEEE Trans. Med. Imaging*, vol. 20, no. 1, pp. 45–57, 2001.
- [41] S. M. Smith, “Fast robust automated brain extraction,” *Hum. Brain Mapp.*, vol. 17, no. 3, pp. 143–155, 2002.
- [42] M. Marjańska, E. J. Auerbach, R. Valabrègue, P. F. Van de Moortele, G. Adriany, and M. Garwood, “Localized <sup>1</sup>H NMR spectroscopy in different regions of human brain in vivo at 7T: T<sub>2</sub> relaxation times and concentrations of cerebral metabolites,” *NMR Biomed.*, vol. 25, no. 2, pp. 332–339, 2012.
- [43] L. Xin, B. Schaller, V. Mlynarik, H. Lu, and R. Gruetter, “Proton T<sub>1</sub> relaxation times of metabolites in human occipital white and gray

- matter at 7 T,” *Magn. Reson. Med.*, vol. 69, no. 4, pp. 931–936, 2013.
- [44] A. Andreychenko, D. W. J. Klomp, R. A. De Graaf, P. R. Luijten, and V. O. Boer, “In vivo GABA T2determination with J-refocused echo time extension at 7 T,” *NMR Biomed.*, vol. 26, no. 11, pp. 1596–1601, 2013.
- [45] R. Kreis, J. Slotboom, L. Hofmann, and C. Boesch, “Integrated data acquisition and processing to determine metabolite contents, relaxation times, and macromolecule baseline in single examinations of individual subjects,” *Magn. Reson. Med.*, vol. 54, no. 4, pp. 761–768, 2005.
- [46] M. Garwood and L. DelaBarre, “The return of the frequency sweep: Designing adiabatic pulses for contemporary NMR,” *J. Magn. Reson.*, vol. 153, no. 2, pp. 155–177, 2001.
- [47] T. W. J. Scheenen, D. W. J. Klomp, J. P. Wijnen, and A. Heerschap, “Short echo time 1H-MRSI of the human brain at 3T with minimal chemical shift displacement errors using adiabatic refocusing pulses,” *Magn. Reson. Med.*, vol. 59, no. 1, pp. 1–6, 2008.
- [48] T. W. J. Scheenen, A. Heerschap, and D. W. J. Klomp, “Towards 1H-MRSI of the human brain at 7T with slice-selective adiabatic refocusing pulses,” *Magn. Reson. Mater. Physics, Biol. Med.*, vol. 21, no. 1–2, pp. 95–101, 2008.
- [49] B. Hubsch, D. Marinier, H. P. Heatherington, D. B. Twieg, and M. W. Weiner, “Clinical MRS Studies of the Brain,” *Invest. Radiol.*, vol. 24, pp. 1039–1042, 1989.
- [50] C. D. Rae, “A guide to the metabolic pathways and function of metabolites observed in human brain 1H magnetic resonance spectra,” *Neurochem. Res.*, vol. 39, no. 1, pp. 1–36, 2014.
- [51] Y. Wu, P. S. Pearce, A. Rapuano, T. K. Hitchens, N. C. De Lanerolle, and J. W. Pan, “Metabolic changes in early poststatus epilepticus measured by MR spectroscopy in rats,” *J. Cereb. Blood Flow Metab.*, vol. 35, no. 11, pp. 1862–1870, 2015.
- [52] R. M. Wellard, R. S. Briellmann, J. W. Prichard, A. Syngienotis, and G.

- D. Jackson, "Myoinositol abnormalities in temporal lobe epilepsy," *Epilepsia*, vol. 44, no. 6, pp. 815–821, 2003.
- [53] F. Riederer *et al.*, "1H magnetic resonance spectroscopy at 3 T in cryptogenic and mesial temporal lobe epilepsy," *NMR Biomed.*, vol. 19, no. 5, pp. 544–553, 2006.
- [54] J. Detour *et al.*, "Metabolomic characterization of human hippocampus from drug-resistant epilepsy with mesial temporal seizure," *Epilepsia*, vol. 59, no. 3, pp. 607–616, 2018.
- [55] R. J. Simister, M. A. McLean, G. J. Barker, and J. S. Duncan, "Proton MR spectroscopy of metabolite concentrations in temporal lobe epilepsy and effect of temporal lobe resection," *Epilepsy Res.*, vol. 83, no. 2–3, pp. 168–176, 2009.
- [56] J. J. Shih, M. P. Weisend, J. A. Sanders, and R. R. Lee, "Magnetoencephalographic and magnetic resonance spectroscopy evidence of regional functional abnormality in mesial temporal lobe epilepsy," *Brain Topogr.*, vol. 23, no. 4, pp. 368–374, 2011.
- [57] E. Achten *et al.*, "Single-voxel proton MR spectroscopy and positron emission tomography for lateralization of refractory temporal lobe epilepsy," *AJNR. Am. J. Neuroradiol.*, vol. 19, no. 1, pp. 1–8, 1998.
- [58] J. Shen, L. Zhang, X. Tian, J. Liu, X. Ge, and X. Zhang, "Use of short echo time two-dimensional <sup>1</sup>H-magnetic resonance spectroscopy in temporal lobe epilepsy with negative magnetic resonance imaging findings," *J. Int. Med. Res.*, vol. 37, no. 4, pp. 1211–1219, 2009.
- [59] M. Y. Xu *et al.*, "Proton MR Spectroscopy in Patients with Structural MRI-Negative Temporal Lobe Epilepsy," *J. Neuroimaging*, vol. 25, no. 6, pp. 1030–1037, 2015.
- [60] M. A. S. Mantoan *et al.*, "Correlation between memory, proton magnetic resonance spectroscopy, and interictal epileptiform discharges in temporal lobe epilepsy related to mesial temporal sclerosis," *Epilepsy Behav.*, vol. 16, no. 3, pp. 447–453, 2009.

- [61] Q. Tan *et al.*, “Quantitative MR spectroscopy reveals metabolic changes in the dorsolateral prefrontal cortex of patients with temporal lobe epilepsy,” *Eur. Radiol.*, 2018.
- [62] S. G. Mueller *et al.*, “Widespread extrahippocampal NAA/(Cr+Cho) abnormalities in TLE with and without mesial temporal sclerosis,” *J. Neurol.*, vol. 258, no. 4, pp. 603–612, 2011.
- [63] J. W. Pan *et al.*, “7T MR spectroscopic imaging in the localization of surgical epilepsy,” *Epilepsia*, vol. 54, no. 9, pp. 1668–1678, 2013.
- [64] D. Wagnerová *et al.*, “The Relationships Between Quantitative MR Parameters in Hippocampus in Healthy Subjects and Patients With Temporal Lobe Epilepsy,” *Physiol. Res*, vol. 64, pp. 407–417, 2015.
- [65] F. Fadaie *et al.*, “<sup>1</sup>H-MRS metabolite’s ratios show temporal alternation in temporal lobe seizure: Comparison between interictal and postictal phases,” *Epilepsy Res.*, vol. 128, pp. 158–162, 2016.
- [66] B. L. Bartnik-Olson, D. Ding, J. Howe, A. Shah, and T. Losey, “Glutamate metabolism in temporal lobe epilepsy as revealed by dynamic proton MRS following the infusion of [U13-C] glucose,” *Epilepsy Res.*, vol. 136, no. July, pp. 46–53, 2017.

## **Chapter 2**

# **7T Magnetic Resonance Spectroscopy of the Hippocampus in Non-Lesional Temporal lobe Epilepsy**

## 2.1 Introduction

Temporal Lobe Epilepsy (TLE) is one of the most common forms of focal epilepsy. Approximately 25-30% of patients with TLE have inadequate control over their seizures with drug treatments and are ultimately diagnosed with medically refractory epilepsy (MRE). Such patients are considered candidates for more invasive treatments such as surgical resection of the affected tissue. While resective surgery has a reasonably high success rate in this cohort, the effectiveness of surgery is diminished in patients without an identifiable structural abnormality on clinical magnetic resonance imaging (MRI) scans to guide the resection [1], [2].

These localization issues are not unique to TLE. One potential technique to help identify epileptic tissue in the MRI-normal population is the use of magnetic resonance spectroscopy (MRS). MRS techniques can discriminate different molecular species present within a tissue of interest using the unique spectral lineshape of each molecule determined by its chemical structure, and measure the concentration of these molecules. Unfortunately, the application of MRS in TLE is hampered by the proximity of many key structures of the temporal lobe, such as the hippocampus, to structures in the head with different magnetic susceptibility to that of the tissue. Specifically, the base of the skull and the sinuses distort the magnetic field produced by the MR system, greatly reducing the signal to noise and overall quality of the resultant spectrum [3]. Most studies which examine metabolites with low MRS signal amplitudes within the temporal lobe have been forced to use either large voxel volumes, leading to ambiguity in the results due to the inclusion of multiple separate brain structures within the same voxel [4], [5], or they have restricted the metabolites under examination to those that can be accurately quantified in spite of poor spectral quality: *N*-acetylaspartate (NAA), total creatine (Cr), and total choline (Cho) [6]–[11].

Several studies have previously examined non-lesional TLE. Decreases in NAA, NAA/Cr, and NAA/(Cr+ Cho) [7], [12]–[15] within the temporal lobe ipsilateral to seizure origin have been most consistently reported, although one study also showed no significant metabolite changes [4]. In addition, some metabolite changes have been found outside the temporal lobe in non-lesional patients using both single voxel MRS and MRS imaging techniques. These studies have shown ipsilateral and extra-temporal decreases in NAA/(Cr+ Cho) [12], [13], [NAA] [16], and *myo*-inositol [4], [16], in addition to variable glutamate behaviour [4], [13]. Resected MRI-normal tissue has also been studied using high resolution magic angle spinning, revealing decreases in glutamate and glutamine and increases in NAA and Cho when comparing non-lesional tissue samples with samples containing hippocampal sclerosis [17].

The use of ultra high field human MRI scanners ( $\geq 7\text{T}$ ) can improve MRS measurements in hard to measure regions of interest such as the hippocampus. The increased main magnetic field strength increases the signal to noise ratio (SNR) of the acquired spectra, while simultaneously increasing spectral dispersion, thereby reducing signal overlap and allowing metabolite signals to be resolved separately. In addition, higher power shim coil amplifiers can better correct field inhomogeneities, thereby improving magnetic field homogeneity within the tissue and consequently spectral quality [18]. The goal of the current study was to examine MRS changes in the hippocampus in TLE patients at 7T to confirm decreases in NAA and increases in Cho concentrations demonstrated by previous studies, while also examining previously hard to measure metabolites such as glutamate, glutamine, and *Myo*-Inositol.

## 2.2 Methods

### 2.2.1 Patient Recruitment

Patients between the ages of 18 and 90 were recruited through the Epilepsy Program at the London Health Sciences Centre. All participants provided informed consent for this study, which was approved by the Western University Health Sciences Research Ethics Board. All patients had been diagnosed with MRI-negative TLE during routine clinical treatment. Prior to recruitment, all patients underwent scalp and/or intracranial electroencephalography (EEG) and a 1.5T MRI scan as part of standard clinical care. Patients were excluded if they were unable to tolerate the 7T MRI scan protocol, if any vascular malformations or tumours were detected on their clinical MRI, or if they suffered from any other significant medical or psychiatric conditions. Age, sex, and handedness matched participants were also recruited to serve as a control group.

In total, 24 patients were recruited, along with 24 healthy controls. Of these, useable data from at least one hippocampus were acquired from 19 patients (14 male, 6 female, average age  $31.8 \pm 11.6$  years) and 20 healthy controls (14 male, 7 female, average age  $32.4 \pm 8.6$  years). MRS data was not collected from the excluded participants either because of hardware issues or because patients could not tolerate the scan due to claustrophobia. Demographic information for all included patients is provided in Table 2.1, including side of seizure localization and duration of epilepsy. Acquired spectra were excluded from analysis if they had a signal-to-noise ratio  $<10$  ( $N=3$ ) and/or if the linewidth was greater than 24 Hz ( $N=2$ ). Full datasets including spectra from both left and right hippocampi were obtained from 15 patients, while only a single useable spectrum was obtained from the remaining four patients. Full datasets were collected from 16 controls, with four controls only providing a single spectrum.



Subject ID	Clinical Seizure Lateralization	Duration of Epilepsy (Years)	Seizure Frequency at Time of Scan	Observed Asymmetry in Concentration Ratios (Left Hippocampus)	Observed Asymmetry in Absolute Concentration (Left Hippocampus)	MRS Seizure Lateralization from Absolute Asymmetry
P01	Right	7	1-2 per mo.	-	↓[NAA], ↓[Cr]	Indeterminate
P03	Left	4	1 per mo.	↑ Glx/Cr	↑[Glx]	Left
P08	Left	1	1 per mo.	-	↑ [Cr]	Left
P10	Right Origin Seizures, Bilateral Spikes	1	3 per yr.	↑ Cho/Cr, ↓ Myo/Cr	↓[Cr], ↓[Cho], ↓[Myo], ↓[Glx]	Right
P12	Left	28	1 per mo.	-	-	-
P13	Right	1	30 per mo.	-	↓[Cho]	Right
P14	Left	5	Sz Free for 1 yr.	-	↓[Cr]	Right*
P15	Right	2	4 per mo.	-	↓[Cho]	Left*
P16	Bilateral	8	4 per mo.	-	↓[Cr], ↓[Myo]	Right
P17	Bilateral	10	7 per mo.	-	-	-
P18	Right	1	17 per mo.	↑ NAA/Cr, ↑ NAA/(Cr+ Cho)	-	-
P19	Right	2	Sz Free for 2 yr.	↓ Cho/Cr	↑[Cr], ↑[Cho]	Left*
P21	Right	1	1 per yr.	-	-	-
P22	Right	1	7 per yr.	-	-	-
P24	Unknown, Bilateral Seizure Spread	1	1 per yr.	-	-	-
P02	Right	2	1 per mo.	Only One Spectrum Collected		
P04	Left	2	8 per mo.	Only One Spectrum Collected		
P09	Bilateral	0.5	4 per yr.	Only One Spectrum Collected		
P23	Bilateral	22	18 per mo.	Only One Spectrum Collected		

**Table 2.1 – Patient Demographics and MRS Asymmetry Results** – Clinical data and MRS results for all patients included in analysis; starred entries in the rightmost column indicate incorrect MRS lateralization. Directionality of metabolite change is based on whether concentration is increased (↑) or decreased (↓) in the left hippocampus relative to the right.

### 2.2.2 Seizure Lateralization

Clinically established seizure lateralization was used in later analyses for classification of MRS spectra. This was determined for each patient as part of clinical treatment, primarily using interictal scalp EEG data and seizure semiology. Additional clinical information such as ictal and/or intracranial EEG was used for lateralization where available.

### 2.2.3 MR Protocol

Due to hardware and software upgrades performed on our 7T MR scanner, two different MR protocols were used over the course of this study.

The first eight patients and eight healthy controls were scanned on a 7T Agilent/Siemens head-only MRI system using a 16 channel transmit and receive birdcage RF head coil (built in house). T<sub>1</sub>-weighted images were collected using an MPRAGE sequence (TE = 2.22 ms, TR = 6.24 ms, voxel size 0.59x0.43x1.00 mm) after global shimming. These images were later used for determining voxel placement. MRS data were acquired using a semi-LASER sequence (TE = 37.5 ms, TR = 3700 ms, 256 averages) from a 2.7x1.3x1.3 cm<sup>3</sup> voxel placed centrally over the hippocampus (See Figure 2.1, row A). This sequence interleaved a water suppressed metabolite spectrum with a metabolite nulled macromolecule spectrum [19], [20]. Metabolite nulling was achieved using a double inversion recovery preparation incorporating two non-selective 5ms adiabatic full passage (AFP) pulses to suppress metabolite signal [18]. Data were obtained from two separate voxels positioned to include the left and right hippocampi. From each voxel we acquired an unsuppressed water spectrum as an internal reference signal for quantification, a full spectrum containing all metabolite and macromolecule resonances using VAPOR water suppression [21], and the previously described macromolecule only spectrum.

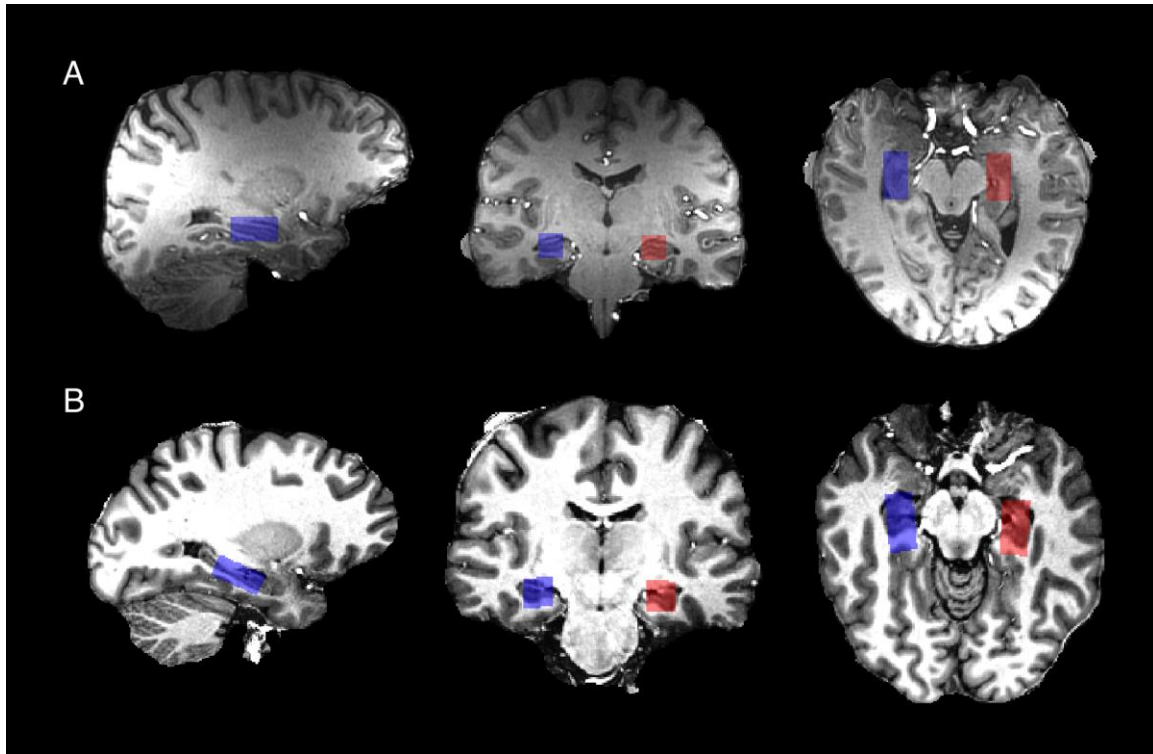


**Figure 2.1 – Hippocampal Voxel Placement:** Image showing voxel placement for A) TE = 37.5 ms acquisition overlaid on a  $T_1$  weighted MPRAGE image and B) a TE = 60 ms acquisition overlaid on a  $T_1$  weighted MP2RAGE image. For the TE= 37.5 ms acquisition, the MRS voxel was placed along the cardinal axes of the MR system, whereas in the TE= 60 ms acquisition the voxel was placed at an oblique angle such that it followed the length of the hippocampus.

The remaining participants were scanned on a 7T Siemens head-only MRI system using a custom built head-only phased array composed of 8 transmit and 32 receive channels. T<sub>1</sub>-weighted images were collected using an MP2RAGE sequence (TE = 2.83 ms, TR = 8.3 ms, voxel size 0.75 mm isotropic). MRS data were collected using a semi-LASER sequence (TE = 60, TR = 7500, 64 averages) from a 2.7x1.3x1.3 cm<sup>3</sup> voxel. This voxel was positioned obliquely along the long axis of the hippocampus (Figure 2.1, row B). From this voxel we acquired an unsuppressed water spectrum and a full spectrum containing metabolite and macromolecule resonances using VAPOR water suppression. This sequence did not incorporate an interleaved macromolecule only acquisition.

#### **2.2.4 Spectral Processing and Metabolite Quantification**

Metabolite levels were measured using custom software developed by our lab. All data first underwent a combination of QUALITY deconvolution, to restore peak Lorentzian lineshape, and eddy current correction. Residual water signals were removed by subtracting an automated Hankel singular value decomposition fit of the water peaks from the acquired spectrum [22], [23]. Metabolite lineshapes were simulated for each pulse sequence using custom software built with PyGamma [24], producing templates that were fitted to the *in vivo* data [25]. The macromolecule only spectra acquired from the healthy controls scanned with TE= 37.5 ms were averaged together to create a template for fitting the macromolecule component. This macromolecule lineshape was added to the prior knowledge templates for data acquired on both MRI systems. The *in vivo* data were then fitted to the simulated metabolite and macromolecule templates in the time domain using a Levenberg-Marquard minimization algorithm to determine the contribution of each metabolite to the in-vivo spectrum [23]. This fitting algorithm established the best possible fit by adjusting peak amplitude for each

metabolite, chemical shift and phase for 5 different groups of metabolites (See Table 2.2), and total spectral linewidth. In total, 14 metabolites were simulated and used to fit the *in vivo* spectrum; these were *N*-acetylaspartate (NAA), *N*-acetylaspartate glutamate, total creatine (Cr), total choline (Cho), lactate, *myo*-inositol (Myo), *scyllo*-inositol, glutamate and glutamine (combined into the measure Glx), glutathione, taurine, glucose, glycine, phosphorylethanolamine, and  $\gamma$ -aminobutyric acid. The concentration for each metabolite was calculated both as a ratio to Cr, and as an absolute concentration using the separately acquired water as an internal reference signal. In addition, NAA/(Cr+ Cho) was calculated for comparison with previous findings in the literature.

Ratios to Cr were calculated by summing the peak amplitudes contributing to each metabolite lineshape, then dividing the normalized metabolite amplitude with that of Cr (see Equation 2.1):

$$X/Cr = \frac{\Sigma S_{Amp,X}}{\Sigma S_{Amp,Cr}} \quad (2.1)$$

where  $X/Cr$  is the ratio of the metabolite of interest X to Cr, and  $\Sigma S_{Amp,X}$  and  $\Sigma S_{Amp,Cr}$  are the total amplitude of all peaks that form the spectral line shape of the metabolite of interest and Cr.

Absolute metabolite levels, which provide average metabolite concentrations within the combined grey/white matter tissue fraction of voxel, were evaluated using the following expression (Equation 2.2):

$$[X]_{Tissue} = \frac{\Sigma S_{Amp,X}}{\Sigma S_{Amp,H_2O}} \frac{n_{\rho,H_2O}}{n_{\rho,X}} \frac{R_{H_2O}}{R_X} * [H_2O]_{Voxel} * (GM + WM) \quad (2.2)$$

where  $[X]_{Tissue}$  is the concentration of the metabolite of interest within the tissue fraction of the MRS voxel,  $\Sigma S_{Amp,X}$  and  $\Sigma S_{Amp,H_2O}$  are the sum of spectral peak amplitudes for the metabolite of interest and water respectively,  $n_{\rho,X}$

and  $n_{\rho,H_2O}$  are the number of protons producing spectral signal for both the metabolite of interest and water,  $R_X$  and  $R_{H_2O}$  are corrections for the combined  $T_1$  and  $T_2$  relaxation of both the metabolite of interest and water (See Table 2.2),  $[H_2O]_{Voxel}$  is the average concentration of water within the voxel (based on GM/WM/CSF tissue fractions), and  $(GM + WM)$  is the voxel tissue fraction for grey and white matter [26].

In all cases, voxel tissue volume fractions were evaluated using the Oxford Centre for Functional MRI of the Brain (FMRIB) software library (FSL) [27]. Images were brain extracted using FSL's Brain Extraction Tool (BET)[28], while GM/ WM/ CSF voxel fractions were determined using the FMRIB Automated Segmentation Tool (FAST) [29]. Literature reported relaxation and water concentration values were used in Equation 2 (See Table 2.2) [30]–[33].

### 2.2.5 Statistical Analysis

Metabolites were excluded from analysis if the coefficient of variation (CV) of their absolute concentration within the healthy control group was greater than 35%. This was done to exclude both metabolites that were not reliably fit by the fitting algorithm, and to exclude metabolites with high variability within a healthy population. The metabolites with CVs below this threshold that were included in the subsequent group comparisons were NAA, Cho, Cr, Myo, and Glx.

For group comparisons, both absolute and relative metabolite concentrations were compared between healthy controls, data from patient hippocampi ipsilateral to clinically established seizure focus, and data from patient hippocampi contralateral to seizure focus. This was accomplished using a pair of MANCOVA tests; one comparing absolute metabolite levels across groups, and the other comparing metabolite ratios. In each test, two

Metabolite	Chemical Shift and Phase Group for Fit	T <sub>1</sub> Grey Matter (s)	T <sub>2</sub> Grey Matter (ms)	T <sub>1</sub> White Matter (s)	T <sub>2</sub> White Matter (ms)	Source
<i>N</i> -Acetylaspartate	NAA	1.83 ± 0.05	191 ± 7	1.90 ± 0.06	164 ± 6	T <sub>1</sub> values from Marjanska et. Al. (2012); T <sub>2</sub> values from Xin et. Al. (2013)
<i>N</i> -Acetylaspartyl Glutamate	NAA	1.21 ± 0.22	191 ± 7	0.94 ± 0.08	164 ± 6	T <sub>1</sub> values from Marjanska et. Al. (2012); T <sub>2</sub> assumed to be the same as <i>N</i> -Acetylaspartate
Lactate	NAA	1.28 ± 0.08	160 ± 20	1.19 ± 0.07	100 ± 15	Assumed same relaxation times as <i>Myo</i> -inositol
Creatine (CH <sub>3</sub> )	Cr	1.74 ± 0.06	131 ± 8	1.78 ± 0.04	113 ± 2	T <sub>1</sub> values from Marjanska et. Al. (2012); T <sub>2</sub> values from Xin et. Al. (2013)
Creatine (CH <sub>2</sub> + NH)	Cr	1.13 ± 0.04	102 ± 3	1.10 ± 0.06	108 ± 5	T <sub>1</sub> values from Marjanska et. Al. (2012); T <sub>2</sub> values from Xin et. Al. (2013)
Choline	Cho	1.51 ± 0.11	200 ± 17	1.32 ± 0.06	139 ± 9	T <sub>1</sub> values from Marjanska et. Al. (2012); T <sub>2</sub> values from Xin et. Al. (2013)
<i>Myo</i> -inositol	Myo	1.28 ± 0.08	160 ± 20	1.19 ± 0.07	100 ± 15	T <sub>1</sub> values from Marjanska et. Al. (2012); T <sub>2</sub> values from Xin et. Al. (2013)
Alanine	Myo	1.28 ± 0.08	160 ± 20	1.19 ± 0.07	100 ± 15	Assumed same relaxation times as <i>Myo</i> -inositol
Glucose	Myo	1.28 ± 0.08	160 ± 20	1.19 ± 0.07	100 ± 15	Assumed same relaxation times as <i>Myo</i> -inositol
Glycine	Myo	1.28 ± 0.08	160 ± 20	1.19 ± 0.07	100 ± 15	Assumed same relaxation times as <i>Myo</i> -inositol
Phosphoryl-ethanolamine	Myo	1.31 ± 0.18	160 ± 20	1.32 ± 0.30	100 ± 15	T <sub>1</sub> values from Marjanska et. Al. (2012); T <sub>2</sub> assumed to be the same as <i>Myo</i> -inositol
<i>Scyllo</i> -inositol	Myo	1.31 ± 0.20	130 ± 20	1.23 ± 0.07	112 ± 4	T <sub>1</sub> values from Marjanska et. Al. (2012); T <sub>2</sub> values from Xin et. Al. (2013)
Taurine	Myo	2.15 ± 0.11	120 ± 20	2.09 ± 0.04	90 ± 16	T <sub>1</sub> values from Marjanska et. Al. (2012); T <sub>2</sub> values from Xin et. Al. (2013)
Glutamate	Glu	1.61 ± 0.09	139 ± 8	1.75 ± 0.04	98 ± 4	T <sub>1</sub> values from Marjanska et. Al. (2012); T <sub>2</sub> values from Xin et. Al. (2013)
Glutamine	Glu	1.64 ± 0.07	139 ± 8	1.74 ± 0.23	98 ± 4	T <sub>1</sub> values from Marjanska et. Al. (2012), T <sub>2</sub> assumed to be the same as Glutamate
Glutathione	Glu	1.14 ± 0.18	80 ± 10	1.06 ± 0.06	97 ± 8	T <sub>1</sub> values from Marjanska et. Al. (2012); T <sub>2</sub> values from Xin et. Al. (2013)
GABA	Glu	1.33 ± 0.16	87 ± 11	1.33 ± 0.16	87 ± 11	Andreychenko et. Al. (2013)
Water	Fit in separate water spectrum	2.00 ± 0.12	48 ± 3	1.55 ± 0.07	47 ± 1	T <sub>1</sub> values from Marjanska et. Al. (2012); T <sub>2</sub> values from Xin et. Al. (2013)

**Table 2.2 – Metabolite Shift Groupings and 7T Relaxation Times used for Absolute Metabolite Quantification**

covariates were used to correct for differences between pulse sequences; one was a categorical variable indicating which system was used to collect the data, and the other was voxel white matter content. White matter content was specifically added to his analysis due to a significant difference in the white matter content between the different voxels used. Statistical analysis was performed in SPSS Statistics (IBM, version 25, 2017).

To determine whether individual metabolites were associated with seizure lateralization, asymmetry indices were calculated for both metabolite ratios and absolute concentrations (Equation 2.3):

$$AI = \frac{[X]_{Left} - [X]_{Right}}{([X]_{Left} + [X]_{Right})/2} \quad (2.3)$$

where  $AI$  is the asymmetry index, and  $[X]_{Left}$  and  $[X]_{Right}$  are the concentrations of the metabolite of interest in the left and right hippocampi respectively [34]. To assess abnormality, the average  $AI$  and its standard deviation were calculated for the healthy control group. Patients were said to have abnormal asymmetry if their asymmetry index for a metabolite fell more than two standard deviations away from the control average. Seizure lateralization was made based on these observed asymmetry abnormalities, and the expected metabolite changes reported in the literature (ipsilaterally, NAA level was expected to decrease, Cho and Cr levels were expected to increase). Asymmetry indices that fell within two standard deviations of the control average were considered non-lateralizing. Average absolute  $z$ -scores were calculated to establish the mean absolute difference in asymmetry between patients and healthy controls.



## 2.3 Results

### 2.3.1 Group Analysis

A typical spectrum acquired from the hippocampus of one participant is provided in Figure 1.6 (pg. 29) along with the fitted metabolite components. In comparison to the primary NAA peak, MRS spectra had an average SNR =  $25.8 \pm 8.2$ , while the average linewidth of the unsuppressed water peak was  $16.8 \pm 3.4$  Hz. The average GM/WM/CSF fractions within hippocampal voxels were  $58 \pm 11\%/36 \pm 13\%/5 \pm 4\%$  for the TE=37.5 ms data and  $65 \pm 5\%/25 \pm 7\%/10 \pm 4\%$  for the TE=60 ms data. Average metabolite levels and ratios for control hippocampi, patient contralateral hippocampi, and patient ipsilateral hippocampi are provided in Table 2.3. For patients with bilateral TLE, both hippocampi were included in the ipsilateral group. When comparing healthy controls to ipsilateral hippocampi to contralateral hippocampi, the MANCOVA analysis showed a significant increase in [Cho] when comparing ipsilateral hippocampi to controls ( $p = 0.03$ ). The MANCOVA did identify and correct for significant differences in the measured concentrations between the TE=37.5 and TE=60 ms pulse sequences; [NAA] was 20% higher in the TE=60 ms data, [Cho] was 17% lower in the TE=60 ms data, [Glx] was 45% higher, NAA/Cr was 41% higher, Myo/Cr was 22% higher, Glx/Cr was 58% higher, and NAA/(Cr+Cho) was 40% higher.

### 2.3.2 Asymmetry Analysis

The results of the asymmetry analysis are summarized in Table 2.4. In patients, there was a high level of asymmetry (average  $|z| = 1.76$ ) in the absolute concentration of Cr in patients compared to healthy controls. When used to lateralize seizure focus, [Cr] increase correctly lateralized seizure focus in 3/12 patients with unilateral seizure focus while also meeting our abnormality criterion of  $>2$  SD from healthy control mean in 1/3 patients

Measure	Control Average and Standard Deviation	Contralateral Patient Average and Standard Deviation	Ipsilateral Patient Average and Standard Deviation	Group Difference <i>f</i> -statistic	Group Difference <i>p</i> -value
<i>N</i> -Acetylaspartate (mM)	11.4 ± 1.9	11.6 ± 3.0	11.5 ± 2.1	0.45	0.64
Creatine (mM)	11.6 ± 1.5	11.9 ± 2.9	11.7 ± 2.5	1.84	0.17
Choline (mM)	3.4 ± 0.5	3.5 ± 0.8	3.9 ± 1.0	3.60	0.03*
<i>Myo</i> -inositol (mM)	6.7 ± 1.4	6.2 ± 2.2	6.8 ± 3.0	0.17	0.84
Glx (mM)	9.8 ± 3.0	8.8 ± 5.9	9.2 ± 4.1	0.06	0.94
NAA/Cr	1.08 ± 0.29	1.03 ± 0.31	1.06 ± 0.38	0.18	0.84
Cho/Cr	0.96 ± 0.13	0.92 ± 0.09	1.00 ± 0.24	1.90	0.16
<i>Myo</i> /Cr	0.80 ± 0.18	0.71 ± 0.24	0.82 ± 0.35	0.90	0.41
Glx/Cr	0.84 ± 0.34	0.77 ± 0.47	0.82 ± 0.46	0.46	0.63
NAA/(Cho+ Cr)	0.55 ± 0.14	0.53 ± 0.15	0.53 ± 0.17	0.39	0.68

**Table 2.3 – Metabolite Levels Within Subject Groups and *p*-values from MANCOVA Analysis:** Average values are given without any corrections for co-varying factors, *p*-values given by main MANCOVA analyses

Measure	Control Asymmetry Average Score	Controls Outside 2 Standard Deviations	Patients with Ipsilat. Increase (>2 SD)	Patients with Ipsilat. Decrease (>2 SD)	Average Patient Absolute Z-Score
<i>N</i> -Acetylaspartate (mM)	-0.03 ± 0.22	1	1	0	0.79
Creatine (mM)	0.16 ± 0.15	0	4	2	1.76
Choline (mM)	0.15 ± 0.15	1	2	1	1.16
Myo-inositol (mM)	0.20 ± 0.42	1	2	1	1.03
Glx (mM)	0.35 ± 0.58	1	2	0	0.72
NAA/Cr	-0.20 ± 0.23	1	0	1	0.72
Cho/Cr	-0.04 ± 0.18	1	1	1	0.87
Myo/Cr	-0.01 ± 0.40	1	1	0	0.80
Glx/Cr	0.23 ± 0.52	0	1	0	0.77
NAA/(Cr+ Cho)	-0.18 ± 0.21	1	0	1	0.83

**Table 2.4 – Average Metabolite Asymmetry Scores and Lateralization Results**

with bilateral TLE (Table 2.1). The other metabolic metrics calculated had lower absolute z-scores and were not as successful at lateralizing seizure origin. For each of these measures, anomalous asymmetry only lateralized one or two of the unilateral patients.

When lateralizing seizure focus using all observed metabolic change in a given subject, metabolite asymmetries successfully lateralized 4/12 unilateral TLE patients, with 3 incorrect lateralizations, and one indeterminate result. For the 4 bilateral TLE patients examined in this analysis, metabolite asymmetry gave an indeterminate result for one patient, and lateralized seizure focus to the right temporal lobe for another.

## **2.4 Discussion**

In this study of non-lesional TLE, we identified a significant increase in the absolute level of Cho in ipsilateral hippocampi from non-lesional TLE patients compared to healthy controls. On an individual basis we found substantial variation in [Cr], which successfully lateralized 3/16 patients using our lateralization criteria of being more than two standard deviations from the mean control level. When corrected for the differences between pulse sequences, we found a significant change in [Cho] levels between groups. Comparing the mean values for [Cho], we see that there is an increase in [Cho] levels ipsilateral to seizure focus relative to control measurements. In the existing literature, changes in Cho have not been previously reported in non-lesional TLE. Increases in choline are associated with cellular membrane turnover, cell density, and gliosis [35], [36]; in studies of epilepsy Cho is commonly included in ratio quantities such as NAA/(Cho+Cr) to sensitize these metrics to increased gliosis, and choline changes have been previously reported by studies examining lesional TLE [2], [6], [10], [37]–[39]. The most common histological finding in MRI-normal TLE is nonspecific gliosis without neuronal damage or loss [2], [7]. With this in mind, our observed changes in

Cho appear to be in agreement with the existing literature, as the known prevalence on gliosis within this patient group is most likely to result in Cho increases [2], [39]. Meanwhile our results did not show a change in NAA levels, the most commonly reported change in the epileptic population [40], [41]. NAA change is typically associated with neuronal dysfunction or loss [18], [36], [42]. As this patient group histologically does not consistently show neuronal damage as in other epilepsies [2], [7], our lack of significant NAA change appears to be consistent with previous research.

The observed variation of [Cr] is also noteworthy. Prior studies have reported metabolite levels as ratios to Cr either due to its assumed invariance between healthy and seizure forming tissue [36], or as a proposed functional measure where a combination of decreases in NAA and increases in Cr created a more powerful measure than the individual metabolites [39], [43]. Our results indicate that in non-lesional TLE absolute [Cr] and [Cho] levels may be more useful than metabolite ratios. While we do not see a consistent ipsilateral change in [Cr] levels between healthy and epileptic tissue, we do see substantial variation in [Cr] levels within patients that is not present in healthy controls. More concerning, this variance in Cr may mask significant changes in other metabolites; we found significant changes in absolute [Cho] levels in our group analysis, however this change was not observed in the Cho/Cr ratio.

One potential factor accounting for the large variance of [Cr] without significant changes in the group analysis is the MRI-negative nature of the patient population. Given the lack of identifiable MRI changes and any histological information, the underlying pathology causing seizures in each patient is unknown. Histology has shown that MRI negative TLE is a heterogeneous group in terms of pathology [2]. It therefore follows that our patient population is heterogeneous in terms of underlying pathology and as

such we would expect patients to have differing metabolic abnormalities. When grouped together, these differing metabolic profiles could very easily average out to no significance, leading to our observed variations in [Cr].

Spectroscopy data for this study were acquired using two different parameter sets for the semi-LASER sequence. Pulse sequence specific simulations were used to account for differences in the metabolite lineshapes arising from differences in echo times. In the MANCOVA analysis, significant differences attributable to the pulse sequences used were found in [NAA], [Cho], [Glx], NAA/Cr, Myo/Cr, Glx/Cr, NAA/(Cr+Cho). These changes can be partially explained by the differing tissue fractions within the different voxels used. The concentrations calculated in our analysis are the average concentration of metabolites within the tissue component of our voxel, as CSF contains negligible metabolite levels, yet the concentration of various metabolites change between grey and white matter. Between our two pulse sequences, 62% of the signal collected during the TE= 37.5 ms acquisition is from grey matter versus a grey matter contribution of 72% for the TE= 60 ms acquisition, with white matter contributing the remaining signal in both cases. NAA, Glu, Myo, and Cr all are present in higher concentrations in grey matter than white matter [18], [36], [44], while Cho levels are higher in white matter than cortical grey matter [45]. These results match with the variations identified by our MANCOVA analysis, where Cho is lower and other metabolites are higher in the TE=60 ms acquisition, with its higher grey matter component.

Several other factors were not controlled for in this study. No corrections were made for the potential impact of anti-epileptic drugs on the MRS results. In addition, time since last seizure at time of scan was not tracked. Seizures have been shown to temporarily cause substantial variation in metabolite levels immediately post-seizure which persist for several hours

post-ictally, making time from last seizure a complicating factor, particularly when examining patients with frequent seizures [46].

## **2.5 Conclusion**

From our analysis, it appears that choline and creatine, as measured independently from one another as absolute quantities, may be biomarkers for epileptic tissue in non-lesional TLE patients. While our results are in general agreement with the existing literature, additional and larger studies, ideally incorporating histological data when available, are necessary to establish the clinical utility of these measures.

## References

- [1] F. Al Sufiani and L. C. Ang, “Neuropathology of Temporal Lobe Epilepsy,” *Epilepsy Res. Treat.*, vol. 2012, pp. 1–13, 2012.
- [2] W. Muhlhofer, Y. L. Tan, S. G. Mueller, and R. Knowlton, “MRI-negative temporal lobe epilepsy—What do we know?,” *Epilepsia*, vol. 58, no. 5, pp. 727–742, 2017.
- [3] T. Breyer *et al.*, “Imaging of Patients with Hippocampal Sclerosis at 7 Tesla. Initial Results,” *Acad. Radiol.*, vol. 17, no. 4, pp. 421–426, 2010.
- [4] R. M. Wellard, R. S. Briellmann, J. W. Prichard, A. Syngeniotis, and G. D. Jackson, “Myoinositol abnormalities in temporal lobe epilepsy,” *Epilepsia*, vol. 44, no. 6, pp. 815–821, 2003.
- [5] R. J. Simister, M. A. McLean, G. J. Barker, and J. S. Duncan, “Proton magnetic resonance spectroscopy of malformations of cortical development causing epilepsy,” *Epilepsy Res.*, vol. 74, no. 2–3, pp. 107–115, 2007.
- [6] K. Ercan, H. P. Gunbey, E. Bilir, E. Zan, and H. Arslan, “Comparative Lateralizing Ability of Multimodality MRI in Temporal Lobe Epilepsy,” *Dis. Markers*, vol. 2016, 2016.
- [7] M. Y. Xu *et al.*, “Proton MR Spectroscopy in Patients with Structural MRI-Negative Temporal Lobe Epilepsy,” *J. Neuroimaging*, vol. 25, no. 6, pp. 1030–1037, 2015.
- [8] D. Wagnerová *et al.*, “The Relationships Between Quantitative MR Parameters in Hippocampus in Healthy Subjects and Patients With Temporal Lobe Epilepsy,” *Physiol. Res*, vol. 64, pp. 407–417, 2015.
- [9] M. F. Chernov *et al.*, “Role of proton magnetic resonance spectroscopy in preoperative evaluation of patients with mesial temporal lobe epilepsy,” *J. Neurol. Sci.*, vol. 285, no. 1–2, pp. 212–219, 2009.
- [10] S. K. Lee, D. W. Kim, K. K. Kim, C. K. Chung, I. C. Song, and K. H. Chang, “Effect of seizure on hippocampus in mesial temporal lobe



- epilepsy and neocortical epilepsy: An MRS study,” *Neuroradiology*, vol. 47, no. 12, pp. 916–923, 2005.
- [11] J. G. Burneo, R. C. Knowlton, E. Faught, R. Martin, S. Sawrie, and R. I. Kuzniecky, “Chronic temporal lobe epilepsy: Spatial extent and degree of metabolic dysfunction studied with magnetic resonance spectroscopy (MRS),” *Epilepsy Res.*, vol. 62, no. 2–3, pp. 119–124, 2004.
- [12] S. G. Mueller *et al.*, “Widespread extrahippocampal NAA/(Cr+Cho) abnormalities in TLE with and without mesial temporal sclerosis,” *J. Neurol.*, vol. 258, no. 4, pp. 603–612, 2011.
- [13] J. . Shen, L. . Zhang, X. . Tian, J. . Liu, X. . Ge, and X. . Zhang, “Use of short echo time two-dimensional  $^1\text{H}$ -magnetic resonance spectroscopy in temporal lobe epilepsy with negative magnetic resonance imaging findings,” *J. Int. Med. Res.*, vol. 37, no. 4, pp. 1211–1219, 2009.
- [14] M. T. Doelken *et al.*, “ $^1\text{H}$ -MRS profile in MRI positive- versus MRI negative patients with temporal lobe epilepsy,” *Seizure*, vol. 17, no. 6, pp. 490–497, 2008.
- [15] J. Suhay *et al.*, “ $^1\text{H}$  MRSI predicts surgical outcome in MRI-negative temporal lobe epilepsy,” *Neurology*, vol. 58, no. 5, pp. 821–823, 2002.
- [16] Q. Tan *et al.*, “Quantitative MR spectroscopy reveals metabolic changes in the dorsolateral prefrontal cortex of patients with temporal lobe epilepsy,” *Eur. Radiol.*, 2018.
- [17] J. Detour *et al.*, “Metabolomic characterization of human hippocampus from drug-resistant epilepsy with mesial temporal seizure,” *Epilepsia*, vol. 59, no. 3, pp. 607–616, 2018.
- [18] R. A. DeGraaf, *in vivo NMR Spectroscopy*, 2nd ed. John Wiley & Sons, Ltd, 2007.
- [19] J. Penner and R. Bartha, “Semi-LASER  $^1\text{H}$  MR spectroscopy at 7 Tesla in human brain: Metabolite quantification incorporating subject-specific macromolecule removal,” *Magn. Reson. Med.*, vol. 74, no. 1, pp. 4–12, 2015.

- [20] M. N. E. Kassem and R. Bartha, “Quantitative proton short-echo-time LASER spectroscopy of normal human white matter and hippocampus at 4 tesla incorporating macromolecule subtraction,” *Magn. Reson. Med.*, vol. 49, no. 5, pp. 918–927, 2003.
- [21] I. Tkáč, Z. Starčuk, I. Y. Choi, and R. Gruetter, “In vivo  $^1\text{H}$  NMR spectroscopy of rat brain at 1 ms echo time,” *Magn. Reson. Med.*, vol. 41, no. 4, pp. 649–656, 1999.
- [22] R. Bartha, D. J. Drost, R. S. Menon, and P. C. Williamson, “Spectroscopic lineshape correction by QUECC: Combined QUALITY deconvolution and eddy current correction,” *Magn. Reson. Med.*, vol. 44, no. 4, pp. 641–645, 2000.
- [23] R. Bartha, D. J. Drost, and P. C. Williamson, “Factors affecting the quantification of short echo in-vivo  $^1\text{H}$  MR spectra : prior knowledge , peak elimination , and filtering,” pp. 205–216, 1999.
- [24] S. a. Smith, T. O. Levante, B. H. Meier, and R. R. Ernst, “Computer Simulations in Magnetic Resonance. An Object-Oriented Programming Approach,” *J. Magn. Reson., Ser. A*, vol. 106, no. 1. pp. 75–105, 1994.
- [25] D. Wong, A. Schranz, and R. Bartha, “Optimized in vivo brain glutamate measurement using long-echo-time semi-LASER at 7 T,” *NMR Biomed.*, 2018.
- [26] R. Rupsingh, M. Borrie, M. Smith, J. L. Wells, and R. Bartha, “Reduced hippocampal glutamate in Alzheimer disease,” *Neurobiol. Aging*, vol. 32, no. 5, pp. 802–810, 2011.
- [27] M. Jenkinson, C. F. Beckmann, T. E. J. Behrens, M. W. Woolrich, and S. M. Smith, “Fsl,” *Neuroimage*, vol. 62, no. 2, pp. 782–790, 2012.
- [28] Y. Zhang, M. Brady, and S. Smith, “Segmentation of brain MR images through a hidden Markov random field model and the expectation-maximization algorithm,” *IEEE Trans. Med. Imaging*, vol. 20, no. 1, pp. 45–57, 2001.
- [29] S. M. Smith, “Fast robust automated brain extraction,” *Hum. Brain*

- Mapp.*, vol. 17, no. 3, pp. 143–155, 2002.
- [30] M. Marjańska, E. J. Auerbach, R. Valabrègue, P. F. Van de Moortele, G. Adriany, and M. Garwood, “Localized  $^1\text{H}$  NMR spectroscopy in different regions of human brain in vivo at 7T:  $T_2$  relaxation times and concentrations of cerebral metabolites,” *NMR Biomed.*, vol. 25, no. 2, pp. 332–339, 2012.
- [31] L. Xin, B. Schaller, V. Mlynarik, H. Lu, and R. Gruetter, “Proton  $T_1$  relaxation times of metabolites in human occipital white and gray matter at 7 T,” *Magn. Reson. Med.*, vol. 69, no. 4, pp. 931–936, 2013.
- [32] A. Andreychenko, D. W. J. Klomp, R. A. De Graaf, P. R. Luijten, and V. O. Boer, “In vivo GABA  $T_2$  determination with J-refocused echo time extension at 7 T,” *NMR Biomed.*, vol. 26, no. 11, pp. 1596–1601, 2013.
- [33] R. Kreis, J. Slotboom, L. Hofmann, and C. Boesch, “Integrated data acquisition and processing to determine metabolite contents, relaxation times, and macromolecule baseline in single examinations of individual subjects,” *Magn. Reson. Med.*, vol. 54, no. 4, pp. 761–768, 2005.
- [34] Y. Aitouche, S. A. Gibbs, G. Gilbert, O. Boucher, A. Bouthillier, and D. K. Nguyen, “Proton MR Spectroscopy in Patients with Nonlesional Insular Cortex Epilepsy Confirmed by Invasive EEG Recordings,” *J. Neuroimaging*, vol. 27, no. 5, pp. 517–523, 2017.
- [35] J. A. Mendes-Ribeiro, R. Soares, F. Simões-Ribeiro, and M. L. Guimarães, “Reduction in temporal N-acetylaspartate and creatine (or choline) ratio in temporal lobe epilepsy: Does this  $^1\text{H}$ -magnetic resonance spectroscopy finding mean poor seizure control?,” *J. Neurol. Neurosurg. Psychiatry*, vol. 65, no. 4, pp. 518–522, 1998.
- [36] C. D. Rae, “A guide to the metabolic pathways and function of metabolites observed in human brain  $^1\text{H}$  magnetic resonance spectra,” *Neurochem. Res.*, vol. 39, no. 1, pp. 1–36, 2014.
- [37] K. N. Fountas, I. Tsougos, E. D. Gotsis, S. Giannakodimos, J. R. Smith, and E. Z. Kapsalaki, “Temporal pole proton preoperative magnetic

- resonance spectroscopy in patients undergoing surgery for mesial temporal sclerosis,” *Neurosurg. Focus*, vol. 32, no. 3, p. E3, 2012.
- [38] J. P. Ranjeva, S. Confort-Gouny, Y. Le Fur, and P. J. Cozzone, “Magnetic resonance spectroscopy of brain in epilepsy,” *Child’s Nerv. Syst.*, vol. 16, no. 4, pp. 235–241, 2000.
- [39] J. W. Pan and R. I. Kuzniecky, “Utility of magnetic resonance spectroscopic imaging for human epilepsy,” *Quant. Imaging Med. Surg.*, vol. 5, no. 2, pp. 313–22, 2015.
- [40] J. W. Pan *et al.*, “7T MR spectroscopic imaging in the localization of surgical epilepsy,” *Epilepsia*, vol. 54, no. 9, pp. 1668–1678, 2013.
- [41] F. Cendes, “Neuroimaging in investigation of patients with epilepsy,” *Continuum (Minneap. Minn.)*, vol. 19, pp. 623–42, 2013.
- [42] R. Kuzniecky *et al.*, “Magnetic resonance spectroscopic imaging in temporal lobe epilepsy - Neuronal dysfunction or cell loss?,” *Arch. Neurol.*, vol. 58, no. 12, pp. 2048–2053, 2001.
- [43] B. Maton, F. Gilliam, S. Sawrie, E. Faught, J. Hugg, and R. Kuzniecky, “Correlation of scalp EEG and 1H-MRS metabolic abnormalities in temporal lobe epilepsy,” *Epilepsia*, vol. 42, no. 3, pp. 417–422, 2001.
- [44] J. W. Pan, T. Venkatraman, K. Vives, and D. D. Spencer, “Quantitative glutamate spectroscopic imaging of the human hippocampus,” *NMR Biomed.*, vol. 19, no. 2, pp. 209–216, 2006.
- [45] P. J. W. Pouwels and J. Frahm, “Regional metabolite concentrations in human brain as determined by quantitative localized proton MRS,” *Magn. Reson. Med.*, vol. 39, no. 1, pp. 53–60, 1998.
- [46] F. Fadaie *et al.*, “1H-MRS metabolite’s ratios show temporal alternation in temporal lobe seizure: Comparison between interictal and postictal phases,” *Epilepsy Res.*, vol. 128, pp. 158–162, 2016.

## **Chapter 3**

### **Conclusion and Future Work**

### 3.1 Conclusions

In this thesis, we aimed to detect metabolite level changes in epileptic tissue using high field magnetic resonance spectroscopy (MRS) in non-lesional TLE patients. To this end, we performed the first single-voxel MRS measurements at a magnetic field strength of 7T in this cohort.

We found that average absolute choline and creatine concentrations were altered in non-lesional TLE patients compared to healthy controls. Similar variations were not found in the commonly used measures NAA/Cr and NAA/(Cr + Cho). The demonstrated alterations were consistent with pre-existing knowledge about non-lesional TLE, suggesting these two metabolites were noteworthy candidates for future metabolic imaging studies. However, levels of these metabolites were not sufficiently different to be useful in seizure lateralization.

There are two primary factors that could be contributing to this poor lateralization ability. Firstly, due to the MRI-normal nature of this patient population we do not have a clear picture of the underlying pathology; differing pathologies would have different metabolic effects, causing the significant but inconsistent changes seen in our results. Furthermore, there is likely a combination of healthy and epileptogenic tissue within our chosen voxel, in varying amounts in each patient. Given that concentration is measured as an average in all the tissue in a voxel, this would dilute any metabolic asymmetries our chosen measurement technique could identify in these patients. Lowering our criteria for determining significant asymmetry could help correct for this partial volume effect. However, lowering the significance threshold also increases the risk that non-pathologic variances in metabolite levels, created either by normal variance in metabolite levels, or by variance in the grey matter/white matter composition of our voxel, would give incorrect seizure lateralization. Another noteworthy confounding factor

for Cho in particular in this regard is diet; Cho levels within the brain are sensitive to the Cho content of food eaten and time since last meal, and dietary Cho fluctuations could be obscuring Cho changes due to epilepsy [1].

In this thesis, we had hoped to demonstrate the clinical utility of 7T MRS. While our conclusions were complicated by changes in scanner hardware and software over the course of our study, based on the data obtained in this study, it does not appear that 7T MRS of the hippocampus in TLE patients provides effective seizure lateralization in the majority of patients. The metabolic changes we detected occurred in metabolites that are readily identifiable at lower field strength. With that said, 7T systems have demonstrated advantages in identifying small lesions in ‘non-lesional’ epilepsy cases [2], and they may have an advantage when performing MRSI or other metabolic imaging techniques which were beyond the scope of this thesis.

### **3.2 Future Work**

The work presented in this thesis could be meaningfully expanded in a number of different ways.

The significant variations in metabolite levels did not provide good lateralization ability in our study. To clearly identify if [Cho] and [Cr] levels are clinically useful in seizure localization, the various confounding factors discussed above should be addressed. To avoid the specificity issues noted with a single voxel measurement, MRSI or other metabolic imaging measurements studying the behaviour of these metabolites as absolute concentrations are needed, as none currently exist in the literature.

Performing such studies at a field strength of 7T could provide the spectral and spatial resolution needed to identify small epileptic foci which elude accurate characterization by single voxel techniques. Ideally, such studies would be paired whenever possible with histopathology of the underlying

tissue, to more clearly identify which metabolites are affected under differing pathologies.

A number of animal studies have shown that Cho dietary supplementation has a neuroprotective effect in rodent models of epilepsy [3]. In light of the Cho changes we have identified, a rodent study that uses MRS to study Cho level change in rodents pre- and post-epileptogenesis with differing levels of dietary Cho could provide useful information on the behaviour of Cho in epilepsy. We found no studies examining the effects of dietary Cho supplementation in the human epileptic population. While a human study examining the effects of dietary choline would be challenging to carry out, if Cho has the same neuroprotective effect in humans as seen in animal models, it could be used to improve the quality of life of intractable epilepsy patients by reducing the cognitive decline seen in these patients.

In the existing literature on epilepsy, very few studies examine the dynamic changes in MRS metabolite levels; the only study found in our review of the literature examining this was a small study of 5 patients [4]. Establishing the clinical utility of MRS requires that any variation in metabolite levels are known and can be controlled for, thus more and larger studies examining post-ictal metabolite changes are needed.

This leads into a common problem with epilepsy studies as a whole; the general lack of large scale, multi-centre studies makes it difficult to demonstrate the clinical utility of MRS in epilepsy. Given that dozens of smaller scale studies conducted over 3 decades have demonstrated that there are metabolic changes occurring in the epileptic population, and that metabolic changes are associated with seizure focus, such a study could provide a powerful case for clinical use of MRS techniques.



## References

- [1] C. D. Rae, “A guide to the metabolic pathways and function of metabolites observed in human brain<sup>1</sup>H magnetic resonance spectra,” *Neurochem. Res.*, vol. 39, no. 1, pp. 1–36, 2014.
- [2] B. G. Santyr *et al.*, “Investigation of hippocampal substructures in focal temporal lobe epilepsy with and without hippocampal sclerosis at 7T,” *J. Magn. Reson. Imaging*, vol. 45, no. 5, pp. 1359–1370, 2017.
- [3] J. K. Blusztajn *et al.*, “Neuroprotective Actions of Dietary Choline,” *Nutrients.*, vol. 9, no. 8, 2017.
- [4] F. Fadaie *et al.*, “<sup>1</sup>H-MRS metabolite’s ratios show temporal alternation in temporal lobe seizure: Comparison between interictal and postictal phases,” *Epilepsy Res.*, vol. 128, pp. 158–162, 2016.

## **Appendix A**

### **Ethics Approval**

## A.1 Ethics Approval for Human Epilepsy study



**Date:** 16 August 2018

**To:** Jorge Burneo

**Project ID:** 6508

**Study Title:** An exploratory study to assess the role of 7T structural and metabolic MR in the evaluation of patients with non-lesional temporal lobe epilepsy

**Application Type:** HSREB Amendment Form

**Review Type:** Delegated

**Full Board Reporting Date:** September 4, 2018

**Date Approval Issued:** 16/Aug/2018

**REB Approval Expiry Date:** 15/Sep/2018

---

Dear Jorge Burneo ,

The Western University Health Sciences Research Ethics Board (HSREB) has reviewed and approved the WREM application form for the amendment, as of the date noted above.

**Documents Approved:**

Document Name	Document Type	Document Date
7T TLE ICF Revision July 30 2018 patients	Consent Form	30/Jul/2018
7T TLE ICF Version July 23 2018 Healthy Controls	Consent Form	23/Jul/2018
7T TLE Protocol Amendment July 23 2018	Protocol	23/Jul/2018

REB members involved in the research project do not participate in the review, discussion or decision.

The Western University HSREB operates in compliance with, and is constituted in accordance with, the requirements of the TriCouncil Policy Statement: Ethical Conduct for Research Involving Humans (TCPS 2); the International Conference on Harmonisation Good Clinical Practice Consolidated Guideline (ICH GCP); Part C, Division 5 of the Food and Drug Regulations; Part 4 of the Natural Health Products Regulations; Part 3 of the Medical Devices Regulations and the provisions of the Ontario Personal Health Information Protection Act (PHIPA 2004) and its applicable regulations. The HSREB is registered with the U.S. Department of Health & Human Services under the IRB registration number IRB 00000940.

Please do not hesitate to contact us if you have any questions.

Sincerely,

Karen Gopaul, Ethics Officer on behalf of Dr. Joseph Gilbert, HSREB Chair

*Note: This correspondence includes an electronic signature (validation and approval via an online system that is compliant with all regulations).*

## **Curriculum Vitae**

# John ADAMS

## EDUCATION

---

- OCT 2018 | Masters of Science, **University of Western Ontario**, London, Canada  
 Medical BioPhysics  
 Thesis: "7T Magnetic Resonance Spectroscopy of the Hippocampus in Non-Lesional Temporal Lobe Epilepsy" | Supervisor: Dr. Robert BARTHA
- MAY 2015 | Bachelor of Science, **University of New Brunswick**, Fredericton, Canada  
 Honours Physics  
 Thesis: "Stimulated Echo Single Point Imaging- A Technique for Quantifying the Small Pore Space in Porous Media" | Supervisor: Dr. Benedict NEWLING  
 GPA: 3.5

## PREVIOUS RESEARCH EXPERIENCE

---

- SEPT 2016 TO  
OCT 2018 | **Masters Thesis at UNIVERSITY OF WESTERN ONTARIO**  
 Under the supervision of Dr. Robert Bartha, in collaboration with Dr. Jorge Burneo, conducted a study on changes in brain metabolism in non-lesional temporal lobe epilepsy patients using magnetic resonance spectroscopy. Was involved in data collection, coding data analysis tools, all data analysis and preparation of relevant manuscripts. Work is currently being prepared for submission to *Epilepsia*. Thesis was successfully defended Oct 2018
- NOV 2014 TO  
APRIL 2015 | **Honors Thesis at UNIVERSITY OF NEW BRUNSWICK**  
 Under the supervision of Dr. Ben Newling, coded and tested the Stimulated Echo Single Point Imaging Pulse (STE-SPI) sequence. This sequence was developed to improve the lab's ability to measure the short  $T_2$  component of the MR signal in spatially resolved rock core porosity measurements. Sequence was shown to measure  $T_2$  decay as short as  $100\mu s$ . Thesis was successfully defended April 2015
- MAY-AUG 2014 | **Summer Student Researcher at UNIVERSITY OF NEW BRUNSWICK**  
 Under the supervision of Dr. Ben Newling, coded and tested MRI pulse programs for measuring slow diffusion in a constant magnetic gradient for use on a GARfield shaped permanent magnet. Two potential pulse sequences, Constant Time Steady Gradient (CTSG) and a 3-pulse sequence, were tested on glycerol and crude oil samples to determine the better pulse sequence for further measurements.
- MAY-AUG 2013  
MAY-AUG 2012 | **Summer Student Researcher at UNIVERSITY OF NEW BRUNSWICK**  
 Under the supervision of Dr. P.T. Jayachandran, wrote and used IDL and Matlab programs to analyse atmospheric data collected by the Canadian High Arctic Ionospheric Network, with the aim of identifying rapid and unusual changes in Ionospheric Total Electron Content (TEC) measurements to guide further research. 2012 research was performed with funding from the NSERC Undergraduate Student Research Award program.

## PREVIOUS TEACHING EXPERIENCE

---

- JAN 2014 TO  
APRIL 2015 | **Private Tutor at UNIVERSITY OF NEW BRUNSWICK**  
 University certified tutor for 1st year physics courses. Provided private and group sessions for private individuals, UNB residences, and the Saint Thomas University Student Accessibility Centre.

---

 SELECTED PRESENTATIONS AND POSTERS
 

---

- JUNE 2018 | John Adams et Al., **7T Magnetic Resonance Spectroscopy of the Hippocampus of MRI Normal Temporal Lobe Epilepsy Patients**, International Society of Magnetic Resonance in Medicine Annual General Meeting, Paris, France, Poster #1355
- APRIL 2018 | John Adams, **7T Magnetic Resonance Spectroscopy of the Hippocampus in MRI-Normal Temporal Lobe Epilepsy Patients**, UWO Department of Clinical Neuroscience Research Day, London, Canada, Oral Presentation
- AUG 2017 | John Adams, **Studying Epilepsy at the Metabolic Level using Magnetic Resonance Spectroscopy**, London Health Sciences Centre Epilepsy Rounds, London, Canada, Oral Presentation
- MARCH 2017 | John Adams et Al., **Metabolic Abnormalities in Epileptic Patients with Malformations of Cortical Development**, Imaging Network of Ontario 2017 Symposium, London, Canada, Poster
- NOV 2016 | John Adams, **Ongoing Studies of Epilepsy using Magnetic Resonance Spectroscopy**, London Health Sciences Centre Epilepsy Research Day, London, Canada, Oral Presentation
- AUG 2015 | Ben Newling and John Adams, **Stimulated-Echo Single-Point Imaging (STE-SPI)**, International Conference on Magnetic Resonance Microscopy, TUM Research Center Garching, Munich, Germany, Poster P-088
- FEB 2015 | John Adams, **STE-SPI: An Improved Magnetic Resonance Method For Analyzing Porosity**, Atlantic Undergraduate Physics and Astronomy Conference, Mount Allison University, Sackville, NB, Oral Presentation
- OCT 2014 | John Adams, **NMR Slow Diffusion Measurements Performed with a Shaped Permanent Magnet**, Canadian Undergraduate Physics Conference, Queen's University, Kingston, ON, Oral Presentation
- FEB 2013 | John Adams, **A Statistical Analysis of the L1 GPS Signal**, Atlantic Undergraduate Physics and Astronomy Conference, Université de Moncton, Moncton, NB, Oral Presentation

---

 EVENT ORGANIZATION
 

---

- JUNE 2018 | **Event Organizer for ROBARTS RESEARCH RETREAT**  
 Robarts Research Retreat is a trainee organized, one day conference which provides the community at the Robarts Research Institute a chance to showcase our research, share our ideas, and learn more about the innovative projects happening within the Institute. In my role as event organizer, I helped with the large scale planning of the event, abstract review and selection, judging assignment, venue layout and poster assignments.